AGU PUBLICATIONS

Tectonics

RESEARCH ARTICLE
10.1002/2014TC003663

Key Points:
- Balanced cross section resolves shortening of ~90 km (30%) in the Pyrenees
- Subduction of 50 km occurred in the earliest stages of convergence (80–70 Ma)
- Rift architecture and inheritance control shortening and onset of exhumation

Supporting Information:
- Readme
- Table S1
- Table S2

Correspondence to:
F. Mouthereau,
frederic.mouthereau@upmc.fr

Citation:
Mouthereau, F., P.-Y. Filleaudeau, A. Vacherat, R. Pik, O. Lacombe, M. G. Fellin, S. Castelltort, F. Christophoul, and E. Masini (2014), Placing limits to shortening evolution in the Pyrenees: Role of margin architecture and implications for the Iberia/Europe convergence, *Tectonics*, *33*, 2283–2314, doi:10.1002/2014TC003663.

Received 23 JUN 2014
Accepted 16 OCT 2014
Accepted article online 21 OCT 2014
Published online 1 DEC 2014

Placing limits to shortening evolution in the Pyrenees: Role of margin architecture and implications for the Iberia/Europe convergence

Frédéric Mouthereau[1,2,3], Pierre-Yves Filleaudeau[4], Arnaud Vacherat[1,2,5], Raphaël Pik[5], Olivier Lacombe[1,2], Maria Giuditta Fellin[6], Sébastien Castelltort[7], Frédéric Christophoul[3], and Emmanuel Masini[8]

[1]Institut des Sciences de la Terre Paris, Sorbonne Universités, Pierre et Marie Curie University Paris 06, UMR 7193, Paris, France, [2]CNRS, UMR 7193, Institut des Sciences de la Terre Paris, Paris, France, [3]Université Toulouse III-Paul Sabatier, Laboratoire Géosciences Environnement Toulouse, UMR 5563, Toulouse, France, [4]Beicip-Franlab, Rueil-Malmaison, France, [5]CRPG-CNRS, Vandoeuvre-lès-Nancy, France, [6]Institute for Geochemistry and Petrology, ETH Zürich, Zurich, Switzerland, [7]Department of Earth Sciences, University of Geneva, Geneva, Switzerland, [8]TOTAL, CTSJF, Pau, France

Abstract Estimating shortening in collision belts is critical to reconstruct past plate motions. Balanced cross-section techniques are efficient in external domains but lack resolution in the hinterland. The role and the original extent of the continental margins during the earliest stages of continental convergence are debated. Here we combine existing and new sequentially restored cross sections in the central Pyrenees, with Iberia/Europe (IB/EU) plate kinematic reconstructions and new apatite fission track, zircon (U-Th)/He, and U/Pb ages to discuss higher and lower bounds of crustal shortening and determine the amount of distal margin sutured during collision. We show that after extension in the Albian (~110 Ma), a 50 km wide extremely thinned crustal domain underwent subduction at 83 Ma. Low-temperature data and thermal modeling show that synorogenic cooling started at 75–70 Ma. This date marks the transition from suturing of the highly extended margin to collision of the more proximal margin and orogenic growth. We infer a relatively low crustal shortening of 90 km (30%) that reflects the dominant thick-skinned tectonic style of shortening in the Pyrenees, as expected for young (Mesozoic) and weak lithospheres. Our proposed reconstruction agrees with IB/EU kinematic models that consider initially rapid convergence of Iberia, reducing from circa 70 Ma onward. This study suggests that plate reconstructions are consistent with balanced cross sections if shortening predicted by age-dependent properties of the continental lithosphere is taken into account.

1. Introduction

Providing constraints on the temporal and spatial evolution of shortening across collision zones is critical to reconstruct past plate motions. In most cases, shortening estimates are retrieved using balanced cross-section techniques in nonmetamorphic, external domains of collisional orogens where precollisional markers are preserved. One main difficulty remains in estimating shortening in collisional setting, and it is due to the poor constraints on the original extent of continental margins and on the original position of the plate boundaries or suture domain.

Strain partitioning during collision is thought to be highly sensitive to the original rift-related rheology and architecture of continental margins [e.g., *Jammes and Huismans*, 2012]. This is particularly obvious for young margins that are dominated by thick-skinned structural style due to age-dependent properties of the continental lithosphere [*Mouthereau et al.*, 2013]. The reactivation and inversion of variably thinned parts of the crust is known to exert a significant control on the early stages of collision (e.g., Alps [*Masini et al.*, 2011; *Mohn et al.*, 2012; *Bellahsen et al.*, 2014], Taiwan [*Mouthereau and Lacombe*, 2006; *Byrne et al.*, 2011; *McIntosh et al.*, 2013; *Mesalles et al.*, 2014], Zagros [*Wrobel-Daveau et al.*, 2010; *Mouthereau et al.*, 2012], and Pyrenees [*Jammes et al.*, 2009; *Lagabrielle et al.*, 2010]). For instance, collision between continental plates characterized by different buoyancies, thermal structure, and rheological stratification shows variable components of underthrusting (subduction) and crustal accretion, which in turn result in a multistage collisional evolution or a complex suturing evolution (e.g., Zagros [*Mouthereau et al.*, 2012] or Taiwan [*Mesalles et al.*, 2014]). Therefore, comparing the collision evolution of an orogen with reconstructions of plate convergence history

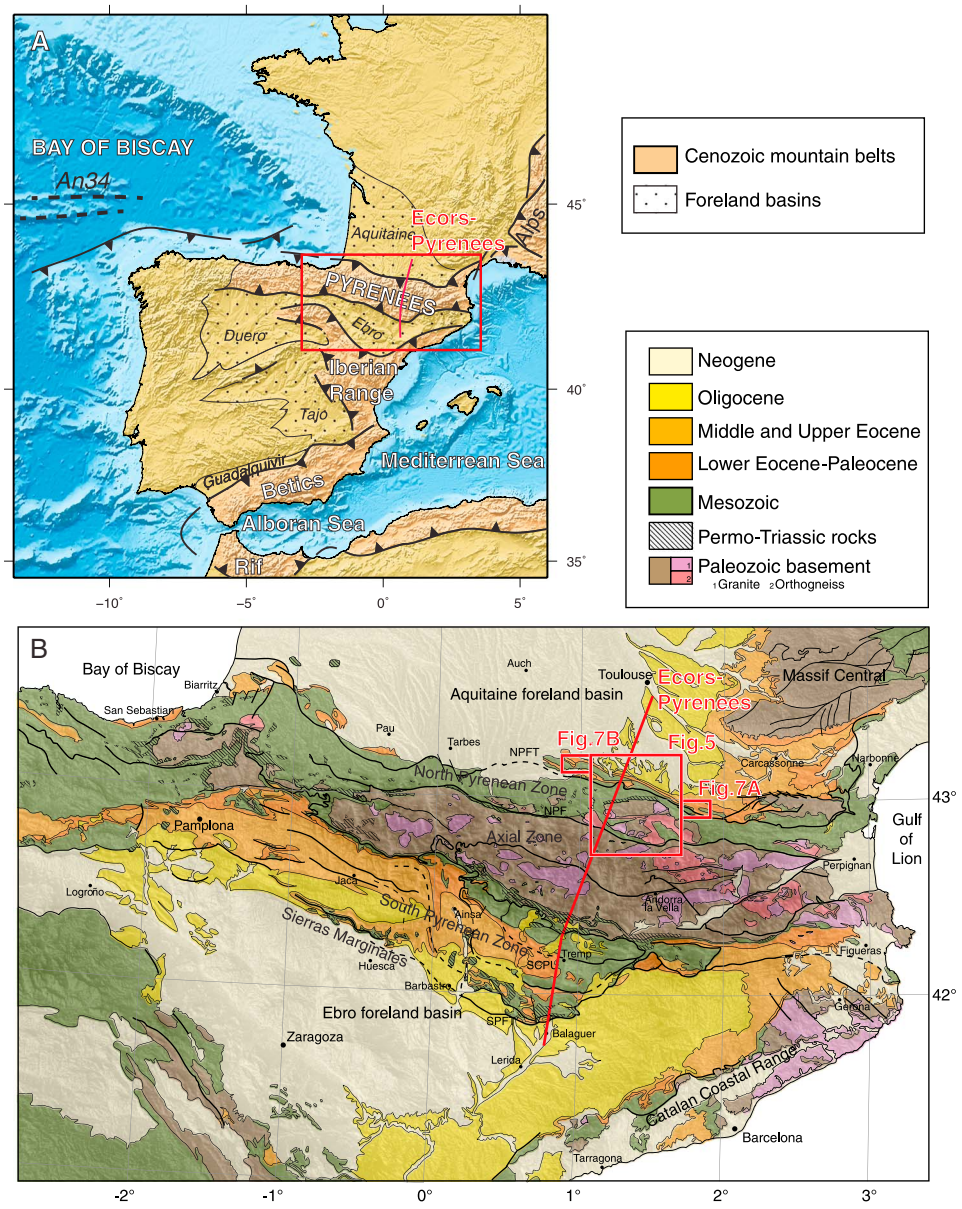

Figure 1. Tectonic and geological framework of the Pyrenees. (a) Main collision-related geological features of the Iberia/Europe collision zone. (b) Geological map of the Pyrenees (after 1 million scale Geological Map of France and the Geological Map of Spain draped on a 3 arc sec digital elevation model). NPF: north Pyrenean Fault, NPFT: north Pyrenean frontal thrust, SCPU: south central Pyrenean thrust unit, SPFT: south Pyrenean frontal thrust. Magnetic anomaly An34 (83 Ma) recognized in Bay of Biscay [*Srivastava et al.*, 1990; *Roest and Srivastava*, 1991] corresponds to change from spreading to collision. From An34 onward Iberia became part of Africa.

requires to carefully evaluate higher and lower bounds of crustal shortening, as inferred from balanced cross-section techniques. This comparison is possible only in regions where proposed plate reconstructions can be tested against well-dated sequential restoration of geological cross sections.

Here we investigate the case of the Pyrenees (Figure 1), which is the result of the collision of the Iberian and European continental margins from Late Cretaceous to late Oligocene [*Choukroune and ECORS-Pyrenees Team*, 1989; *Roure et al.*, 1989; *Roure and Choukroune*, 1998; *Beaumont et al.*, 2000]. Positioned between the Atlantic and the western Tethyan domains, the kinematics of plate boundaries surrounding the Iberian Plate during the Aptian-Albian extension, and subsequent movement in the Cretaceous, are strongly debated [*Olivet*, 1996; *Sibuet et al.*, 2004; *Jammes et al.*, 2009; *Vissers and Meijer*, 2012a, 2012b].

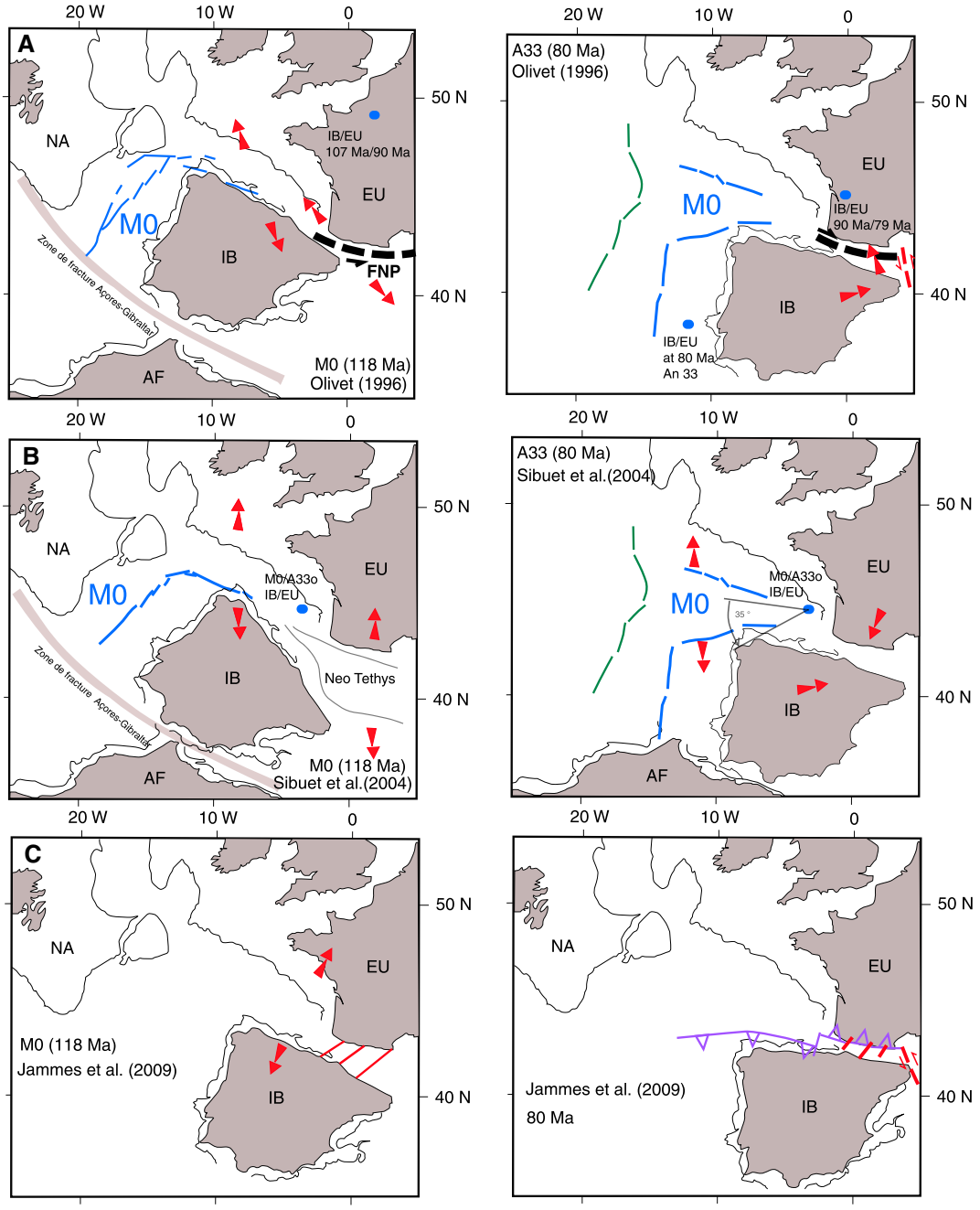

Figure 2. Proposed kinematic reconstructions of Iberia motion in the Lower Cretaceous (*M*0 anomaly ~118 Ma) and at onset of convergence in Late Cretaceous (anomaly An33 at 80 Ma). (a) Transtensional rift model after *Olivet* [1996], which accounts for dextral strike-slip reactivation and inversion of the Iberian and European margins during oblique convergence. (b) Kinematic reconstruction of Mesozoic motion of Iberia after *Jammes et al.* [2009] that includes transcurrent motion of Iberia during the Late Jurassic, followed by orthogonal stretching in the Middle-Late Cretaceous, and subsequent frontal convergence of Iberia. (c) Scissor opening model after *Srivastava et al.* [2000] that implies large oceanic subduction beneath the Pyrenees during the Albian. The position of North America (NA), Africa (AF), and Iberia (IB) relative to fixed Eurasia (EU) is shown as well as location of IB/EU rotation poles (blue circles). Anomaly A33 and *M*0 are shown as green and blue segments, respectively.

Three types of models are generally proposed (Figures 2a–2c). A transtensional rift model (Figure 2a), which involves a significant component of dextral strike-slip reactivation and inversion of the Iberian and European margins during oblique convergence [*Choukroune and Mattauer*, 1978; *Savostin et al.*, 1986; *Olivet*, 1996]. The scissor opening model (Figure 2b) implies a significant subduction beneath the Pyrenees synchronous with

the opening in the Bay of Biscay during the Albian [*Srivastava et al*., 1990; *Sibuet et al*., 2004; *Vissers and Meijer*, 2012a, 2012b]. A third model (Figure 2c) accounts for transcurrent motion of Iberia during the Late Jurassic (Tithonian ~147 Ma) [*Schettino and Turco*, 2010], arc-normal (orthogonal) stretching in the Middle-Late Cretaceous, and the subsequent frontal convergence of Iberia [*Jammes et al*., 2009]. All these models assume contrasting amounts of subduction of oceanic/transitional crust (0 to 400 km) and continental crust (0 to more than 100 km). The role of the Mesozoic North Pyrenean Fault, a strike-slip plate boundary fault, is also questioned. In the first model, the North Pyrenean Fault (NPF) plays an important role. It is a transform fault boundary that localizes eastward displacement of Iberia during the Aptian-Albian. In this model, Iberia also took part of the plate reorganization into the Alpine Tethys and Adria Plate domain, leading to the Eo-Alpine orogen and subduction of Iberia below Adria [*Handy et al*., 2010]. In the second model, the NPF strike slip is only active during the collision from 83 Ma onward and plays a minor role by accommodating the strike-slip component of the convergence. In the third model, the NPF accommodates about 400 km of eastward displacement of Iberia relative to Europe during the Late Jurassic to Aptian. As a result, Iberia has virtually no movement to the east after the Late Jurassic and therefore has no role during the early stages of the Eo-Alpine orogeny.

Despite an apparent consensus on the total amount of Iberia plate convergence, which is about 180 km since 83 Ma [*Olivet*, 1996; *Rosenbaum et al*., 2002; *Sibuet et al*., 2004; *Vissers and Meijer*, 2012a], current interpretations of the structure of the central Pyrenees imply different amount and temporal distribution of shortening. For instance, *Beaumont et al*. [2000] estimate shortening of 165 km, while *Roure et al*. [1989] propose 100 km. This outlines the different views of crustal shortening processes in the Pyrenees. The main difference lies in the vertical distribution of shortening. While *Roure et al*. [1989] assume the stacking of the whole Iberian crust above a detachment in the lower crust (thick-skin style of deformation), *Beaumont et al*. [2000] suggest a prominent subduction of the whole crust beneath the Axial Zone (thin-skin style of deformation).

Hyperextension of the European margin during the Aptian-Albian is thought to have led to widespread exhumation of the subcontinental mantle along the strike of the Pyrenees [*Jammes et al*., 2009; *Lagabrielle et al*., 2010]. Preorogenic extension is also argued by the occurrence of ductile extensional shear zones active during the formation of the Albian basins [*Vauchez et al*., 2013]. This tectonic event was associated with a regional thermal anomaly, as revealed by the age of high-temperature (HT) metamorphism and K magmatism. Of particular interest for the early tectonic evolution of the Pyrenees is whether the anomaly was still present during the onset of shortening.

Apatite fission track (AFT) thermochronology in the Pyrenees suggests onset of significant exhumation at 55 Ma [*Fitzgerald et al*., 1999]. However, detrital zircon fission track (ZFT) and (U-Th)/He thermochronology in the southern Pyrenees [*Beamud et al*., 2011; *Filleaudeau et al*., 2011; *Rahl et al*., 2011; *Whitchurch et al*., 2011], including modeling of AFT data on granitic cobbles [*Beamud et al*., 2011] allowed to resolve an earlier collision event circa 70 Ma. Independent plate reconstructions argue that the onset of convergence between Iberia and Europe started at least in the Santonian, at ~83 Ma [*Roest and Srivastava*, 1991; *Olivet*, 1996; *Rosenbaum et al*., 2002]. The apparent mismatch between the timing of initiation of plate convergence and collision/shortening-related cooling age may express the time needed to erode the nonreset part of the crust, depending on the initial crustal thickness and rates of shortening. It may otherwise reflect a change in the thermal structure of the crust as convergence involves successively a hot and extremely thinned crust at distal margin, where extension was the largest, followed by a cooler and thicker crustal portion of the proximal margin. This emphasizes the need to gain better resolution on the timing of cooling and/or exhumation during the earliest stages of collision. Low-temperature thermochronological data are available mainly for the southern Pyrenees. We therefore lack key elements to understand the whole cooling history of the Pyrenees and also the resolution of the integrated kinematic picture. Confronting new time-temperature constraints from northern Pyrenees with plate kinematics and sequentially restored geological cross sections is required to advance on the role of rift-related margin architecture.

To this aim, we develop an approach in which shortening data derived from balanced cross-section techniques are used in combination with plate kinematic constraints and new detrital AFT and zircon (U-Th)/He (ZHe) ages from the northern Pyrenees. This material is used to propose a restoration of the suture zone in the central Pyrenees.

2. The Pyrenean Collision: Overview of Geodynamic and Geological Setting and Main Issues

2.1. Iberia/Europe Plate Motion: Inconsistencies Between Plate Kinematics and Geological Constraints

Main critical issues regarding the collision period in the Pyrenees account for existing uncertainties on the Iberia plate position relative to Europe (Figure 2). The position of the Pyrenean domain during the Variscan orogeny is poorly constrained, although the structure and stratigraphy of the Variscan units in the Pyrenees are relatively well defined [*García-Sansegundo et al*., 2011]. The collapse of the Variscan orogeny during the Permian-Trias [*Vissers*, 1992; *Vissers and Meijer*, 2012a] was followed in the Late Jurassic by rifting in the Alpine Tethys [*Choukroune*, 1992] and by opening of central Atlantic domain [*Schettino and Turco*, 2010], which is recorded in the subsidence patterns of Mesozoic basins in the Pyrenees and Bay of Biscay [*Vergés and García-Senz*, 2001; *Biteau et al*., 2006]. A second stretching phase spans the Barremian to Albian (130–112 Ma) leading during the Aptian to break up in the Bay of Biscay [*Olivet*, 1996; *Vergés and García-Senz*, 2001]. Because Iberia moved relative to Europe from the end of the M0 anomaly (118 Ma) throughout the Cretaceous Normal Superchron (C34), there are no seafloor anomalies to constrain its position.

In a first attempt to reconstruct plate motions *Le Pichon and Sibuet* [1971], *Choukroune et al*. [1973], and *Choukroune and Mattauer* [1978] later updated by *Olivet* [1996] and *Fidalgo González* [2001], interpreted the Cretaceous basins observed in the Pyrenees to be pull-apart basins, accommodating distributed continental extension along a major transcurrent plate boundary fault, the North Pyrenean Fault (NPF; Figures 1 and 2a). The NPF is assumed to be transtensional to purely strike slip associated with polyphase rifting from Barremian (127 Ma) up to the Coniacian (~90 Ma) [*Olivet*, 1996]. From the Middle Albian to the Coniacian, the rotation pole is located on the European Plate, leading to significant sinistral strike-slip motion. The amount of rotation of Iberia induced by this reconstruction and paleomagnetic analyses [*Gong et al*., 2008] range between 27° and 35° during the Aptian (121–112 Ma), which is not taken into account in earlier reconstructions by *Olivet* [1996].

In addition, while *Olivet* [1996] relies upon the "*J*" anomaly between Iberia and Newfoundland, the scissors-like opening model of the Bay of Biscay (Figure 2b) is based on the perfect fitting of *M*0 magnetic anomaly between Iberia and Newfoundland [*Srivastava et al*., 1990, 2000; *Sibuet et al*., 2004; *Vissers and Meijer*, 2012a]. Contrary to previous models, the rotation of Iberia occurred between 118 Ma and 80 Ma. The IB/EU pole being located to the west of the Pyrenees, a significant subduction occurred during the Albian south of the Pyrenees [*Sibuet et al*., 2004] because geological constraints show that extension prevailed at this time in the Pyrenees [*Dinarès-Turell and García-Senz*, 2000; *García-Senz*, 2002], *Sibuet et al*. [2004] inferred back-arc extension. *Vissers and Meijer* [2012b] suggested that subduction of oceanic to transitional lithosphere of the Neotethys occurred at 120 Ma in the Pyrenees. This implies a North directed subduction of a large Neotethyan oceanic domain that is incompatible with current reconstructions of the Alpine Tethys [*Manatschal*, 2004; *Handy et al*., 2010; *Schettino and Turco*, 2010].

The third model (Figure 2c) is intended to better account for processes of extension at magma-poor continental margins [*Jammes et al*., 2009]. In this regard, the occurrence of ultramafic bodies in the Pyrenees in rifted basins, a well-known example of "orogenic peridotites" [*Bodinier and Godard*, 2007], is used to argue that the subcontinental mantle was tectonically emplaced in the Albian during extreme crustal thinning. Continent extension occurred contemporaneously with oceanic accretion in the Bay of Biscay and rotation of Iberia in the Aptian [*Gong et al*., 2008]. In this model, the accommodation of the eastward motion of Iberia of 300–500 km relative to Europe was taken up by extension between Newfoundland and Iberia margins in the Late Jurassic and the Lower Cretaceous. This is a major difference with respect to *Vissers and Meijer* [2012b], in which mantle exhumation is thought to have occurred between the Jurassic and the Barremian.

For *Srivastava et al*. [2000], the convergence began with the Cretaceous Normal Superchron (118 Ma), while reconstruction proposed by *Olivet* [1996] suggests that the onset of convergence and the collision are nearly coeval with the end of Cretaceous Normal Superchron (83 Ma). In agreement with geological data showing that the Pyrenean domain started to be contractional by late Santonian, both models agree that convergence (including a component of strike-slip movement or not) was ongoing at ~83 Ma (chron C33). This is consistent with the end of oceanic accretion in the Bay of Biscay. They, however, imply different component of total plate convergence ranging from 100 km [*Olivet*, 1996] to up to 400 km or more [*Srivastava et al*., 2000; *Rosenbaum et al*., 2002; *Vissers and Meijer*, 2012b].

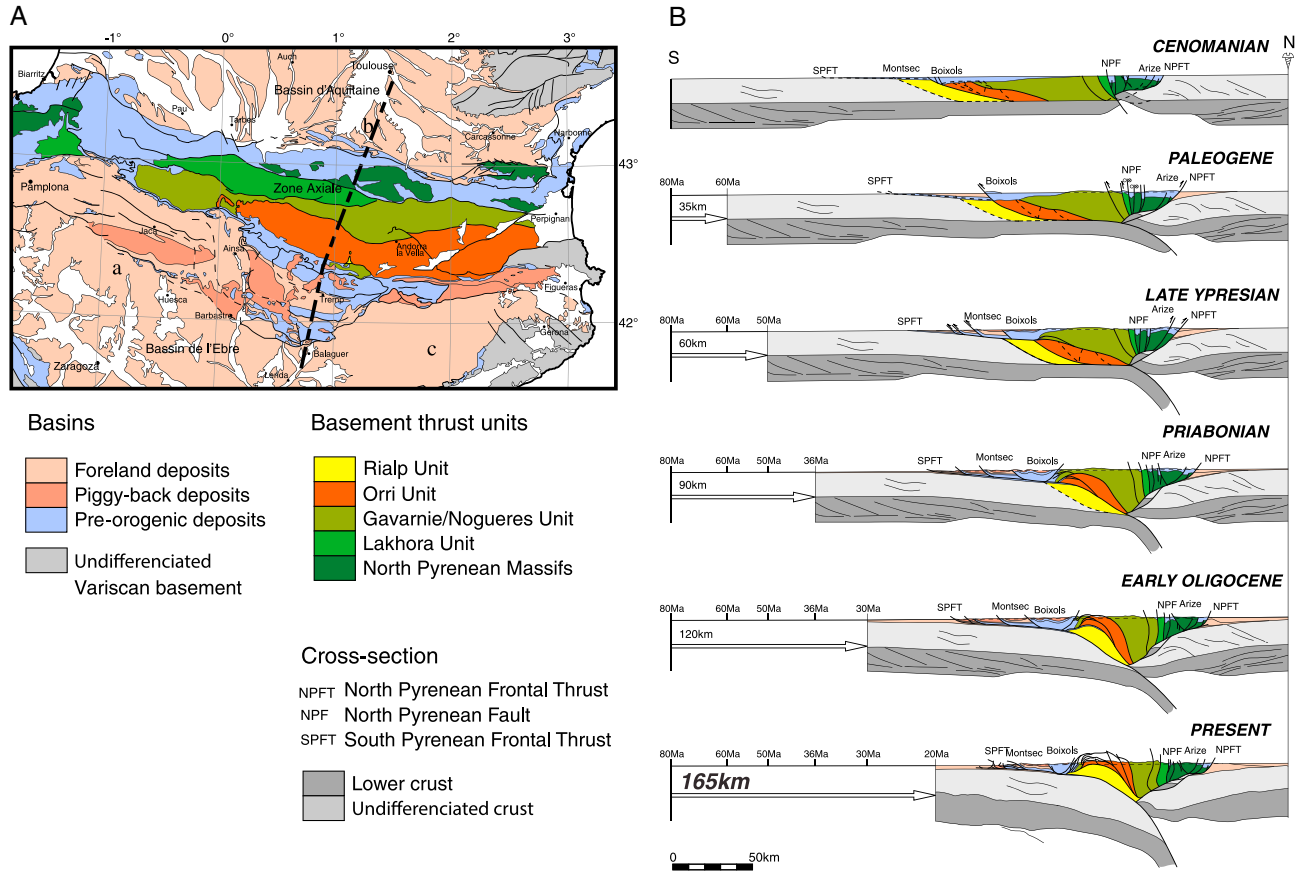

Figure 3. Tectonic division and evolution of central Pyrenees assuming 165 km of shortening. (a) Main thrust sheets in the Pyrenees with distinction of preorogenic and synorogenic basins. (b) Sequential restoration of the central Pyrenees after *Beaumont et al.* (2000). Shortening is reconstructed by progressive restoration of the originally continuous and undeformed Cenomanian reference level. Note that restoration in the preorogenic configuration (Cenomanian) considers a narrow rift zone centered on the northern Pyrenees with no breakup of the crust. Also, note the significant internal shortening of the Gavarnie/Nogueres units, as well as the occurrence of south vergent Variscan thrust ramps in the lower crust of Iberia and European upper crust.

Available estimates of shortening across the Pyrenees based on North-South balanced geological sections [*Choukroune and ECORS-Pyrenees Team*, 1989; *Roure et al.*, 1989; *Teixell*, 1998; *Vergés et al.*, 2002; *Martinez-Peña and Casas-Sainz*, 2003] increase eastward from 75 km to 125 km, with a maximum of 165 km in the central Pyrenees [*Beaumont et al.*, 2000] (Figure 3). Because plate reconstructions account for a homogeneous convergence of 180 km along strike since 83 Ma [*Rosenbaum et al.*, 2002], the difference in crustal shortening resolved from balanced cross sections should indicate variable amount of subduction. This could reflect lateral changes in the architecture of the continental margins at onset of IB/EU convergence. For instance, the early stages of convergence may include prominent thin-skin continental accretion at distal hyperextended crust. Conversely, thick-skin collisional-style deformation reflects distributed shortening of more proximal domains of the Mesozoic continental margin in agreement with shortening style in external parts of collisional orogens [e.g., *Mouthereau et al.*, 2013].

The temporal evolution of shortening established for the Pyrenees [e.g., *Beaumont et al.*, 2000] includes a period of accelerated contraction between 30 and 20 Ma. During this period 45 km of convergence were accommodated in the southern Pyrenees as indicated by the subduction of the Iberia basement (Figure 3). This acceleration, positioned at the end of the collision, is difficult to integrate in classical kinematic evolution of collisional orogens, in which plate convergence rates decrease or stabilize in the course of collision (e.g., Himalaya [*Molnar and Stock*, 2009; *Copley et al.*, 2010]). The increasing resistive forces opposed to forces driving plate at the origin of the slowing of plate motion. Moreover, the increase of potential energy in the upper plate related to mountain building and buoyancy forces are recognized as prime factors. In the case of the Pyrenees, plate reconstructions show either decreasing rate of IB/EU convergence after 33–35 Ma

[*Fidalgo González*, 2001], increasing [*Vissers and Meijer*, 2012a] or constant rates since ~50 Ma [*Rosenbaum et al*., 2002]. The long-term rates of thrust propagation are also expected to diminish in order to maintain the balance of forces necessary for the growth of the mountain belt [*DeCelles and DeCelles*, 2001].

In an effort to propose a suitable plate circuit, *Vissers and Meijer* [2012a] showed that a combination of finite reconstruction poles is needed to be consistent with geological reconstructions of *Beaumont et al*. [2000]. These difficulties reveal the limitations of using a single cross section to validate plate kinematic reconstructions. For instance, most structural and stratigraphic analyses used in existing cross sections, including subsurface data that have been used to build cross sections, were obtained in the southern Pyrenees. The northern Pyrenees therefore lacks chronological constraints, and especially those relevant to the early stage of shortening. Moreover, there are uncertainties on internal deformation of the Iberian plate away from the Pyrenees that are not taken into consideration in existing plate reconstructions. A better definition of the range of shortening values and timing of crustal accretion that examine the role of the margin architecture is therefore required to discuss the validity of plate reconstructions.

2.2. Tectonostratigraphic and Thermotectonic Evolution of the Pyrenees

The Pyrenean mountain belt consists of stacked Iberian and European crustal units forming an asymmetric doubly vergent orogenic wedge [*Séguret*, 1972; *Choukroune and ECORS-Pyrenees Team*, 1989; *Roure et al*., 1989; *Muñoz*, 1992; *Beaumont et al*., 2000]. It can be divided into two opposite vergent thrust belts, the South and the North Pyrenean zones, and a basement core, the Axial Zone (Figures 1 and 3). In the following, we describe in details the thermotectonic and stratigraphic evolution of the central part of the Pyrenees, parallel to the ECORS section.

2.2.1. The Axial Zone

The Axial Zone is formed by southward propagating crustal thrust units named, from bottom (south) to top (north), Rialp, Orri, and Gavarnie-Nogueres (Figures 1 and 3) [e.g., *Muñoz*, 1992]. These units are composed of slightly metamorphosed, thick Paleozoic sedimentary clastic succession, and magmatic units. The Paleozoic series are intruded by Late Variscan (Carboniferous)-Permian granitoids [*Vissers*, 1992; *Deloule et al*., 2002; *Laumonier et al*., 2004; *Castiñeiras et al*., 2008; *Denèle et al*., 2009]. Late Cadomian and Ordovician magmatic rocks are also present, especially in the eastern Pyrenees and in the North Pyrenean Zone (NPZ). The intense Variscan cleavage is overprinted by Alpine cleavage in the North Pyrenean domain, in the vicinity of the NPF and at the transition between the Axial Zone and the southern Pyrenean thrust belt [*Choukroune and Séguret*, 1973].

Thanks to the numerous bedrock low-temperature thermochronological studies, the timing of thrust-related exhumation in the Pyrenees, from east to west, is well constrained for the Eocene-Oligocene [*Morris et al*., 1998; *Fitzgerald et al*., 1999; *Sinclair et al*., 2005; *Gibson et al*., 2007; *Jolivet et al*., 2007; *Maurel et al*., 2008; *Metcalf et al*., 2009]. Figure 4 shows a synthesis of available low-temperature thermochronological, both detrital and in situ, across the orogen. They show a southward younging of AFT and apatite (U-Th)/He (AHe) ages from 50–40 Ma to 20 Ma, revealing an asymmetric orogenic-related exhumation pattern in the central Pyrenees [*Fitzgerald et al*., 1999]. A noticeable acceleration of exhumation in the Axial Zone is reported in the late Eocene to early Oligocene (37–30 Ma) [*Fitzgerald et al*., 1999; *Fillon and van der Beek*, 2012]. The cause for this increase in erosion rates is debated. It could be related to an acceleration of IB/EU plate convergence but the late Eocene to early Oligocene period shows declining convergence rates in this region [*Jolivet and Facenna*, 2000]. Therefore, it has been argued that faster erosion may reflect a component of climatic forcing [*Huyghe et al*., 2009]. Alternatively, temporal consistency of the increase in erosion rates in the central Pyrenees with the transition toward postorogenic extension and slab retreat in the western Mediterranean Sea [*Dewey et al*., 1989; *Jolivet and Facenna*, 2000] may suggest a causal correlation.

2.2.2. The South Pyrenean Thrust Belt

The South Pyrenean Zone (SPZ) forms a typical fold-thrust belt made of Mesozoic sediments detached in the Triassic evaporites (Figures 1 and 3). Thrust sheets propagated southward, within the foreland basin, individualizing piggyback basins. The thrust sequence initiated during the Campanian ~72 Ma, with the inversion of the Aptian-Albian Organyà Basin and Boíxols thrust [*Bond and McClay*, 1995; *Rahl et al*., 2011] and exhumation of the Gavarnie-Nogueres unit in the Axial Zone [*Filleaudeau et al*., 2011; *Whitchurch et al*., 2011]. Older ZHe cooling ages recovered from the Late Cretaceous sandstones suggest that cooling may have started earlier in the Late Santonian (~84 Ma) [*Filleaudeau et al*., 2011] (Figure 4). Tectonostratigraphic

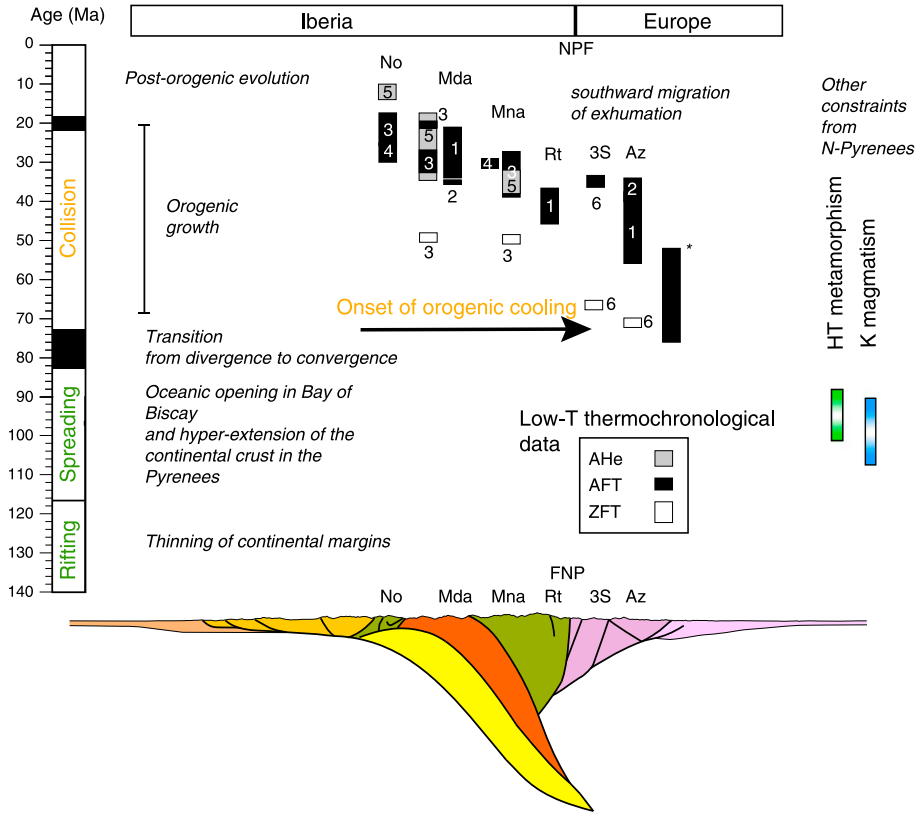

Figure 4. Synthesis of bedrock cooling ages and ages of K magmatism and high-temperature metamorphism plotted against main tectonic events. Thermochronometers are apatite (U-Th)/He (AHe), apatite fission tracks (AFT), zircon (U-Th)/He (ZHe), and zircon fission tracks (ZFT). No: Nogueres, Mda: Maladeta, Mna: Marimaña, Rt: Riberot, 3S: Trois-Seigneurs, Az: Arize. Age constraints are from (1) *Fitzgerald et al.* [1999] (2) *Morris et al.* [1998], (3) *Sinclair et al.* [2005], (4) *Jolivet et al.* [2007], (5) *Gibson et al.* [2007], and (6) *Yelland* [1991] and compilation from *Whitchurch et al.* [2011]. Cross section with main tectonic units is shown with the same color code as in Figure 3.

relationships in the Cotiella Massif further reveal southward inversion of the extensional fault system at this time [*McClay et al.*, 2004], coeval with the movement of the Riberot or Eaux-Chaudes/Lakhora units in the north.

As plate convergence accelerated, activity of the Nogueres unit resumed during the late Ypresian and early Lutetian ~48 Ma [*Farrell et al.*, 1987; *Poblet et al.*, 1998]. This is marked by the development of the Montsec ramp and the wedge-top Tremp-Graus Basin. Both detrital ZFT [*Whitchurch et al.*, 2011] and detrital AFT ages [*Beamud et al.*, 2011] consistently indicate growth of the Axial Zone topography at circa 50 Ma, with exhumation rates of ~0.2 km/Myr. A paleoelevation study shows that the Pyrenees were uplifted up to an altitude of about 2000 ± 500 m at that time (49–41 Ma) [*Huyghe et al.*, 2012a]. At the Lutetian-Bartonian boundary (~40 Ma), the last carbonate platform disappeared and was replaced by foreland siliciclastic deposition [*Huyghe et al.*, 2012b]. The final stage of deformation occurred between 37 Ma and ~25 Ma in the Sierras Marginales [*Meigs et al.*, 1996]. At this time, the out-of-sequence Morreres back thrust onto the southern Axial Zone was active, and the Orri and Rialp units exhumed [*Beamud et al.*, 2011]. Exhumation rates in the Axial Zone accelerated up to 2–4 km/Myr at 35–30 Ma, as inferred from AFT data [*Fitzgerald et al.*, 1999] or 1–1.5 km/Myr at 31–29 Ma from AHe ages [*Gibson et al.*, 2007]. Detrital ZFT ages show cooling at 30 Ma and short lag times, indicating rapid exhumation rates up to 3–4 km/Myr [*Whitchurch et al.*, 2011]. Starting in the late Priabonian (37–35 Ma), the onset of rapid cooling in the Axial Zone overlaps with the continental-to-marine transition of the sedimentation in the Ebro Basin at 36 Ma [*Costa et al.*, 2010]. The increased sediment supply resulted in the accumulation of continental conglomerates, up to 1.6 km [*Fillon et al.*, 2013], aggrading onto the southern fold-thrust belt and the Axial Zone [*Mellere*, 1993; *Coney et al.*, 1996; *Babault et al.*, 2005]. From 31 to 24 Ma, exhumation progressively slowed down in the Axial Zone [*Beamud et al.*, 2011]. A late postorogenic burial and exhumation at 20–5 Ma is then recorded

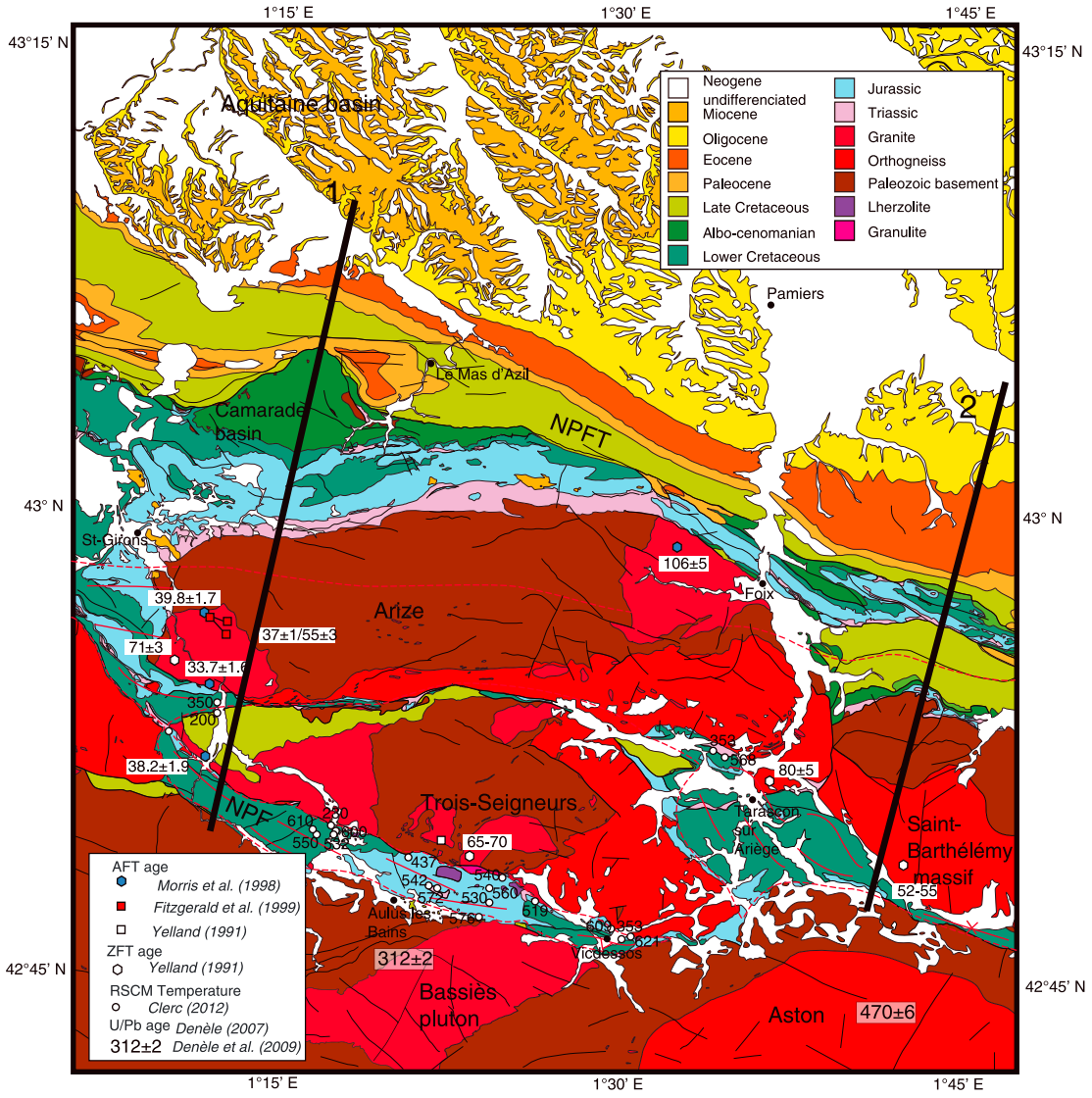

Figure 5. Geological map of the northern central Pyrenees (see location in Figure 1). Low-temperature thermochronological constraints from apatite and fission track data and U/Pb ages from Bassiès pluton and Aston Massif are shown. The map was established from compilation of 50,000 scale maps.

only by few in situ AFT and AHe in the Axial Zone [*Gibson et al.*, 2007; *Jolivet et al.*, 2007], by detrital AFT and AHe data in the SPZ [*Fillon and van der Beek*, 2012] and in central and eastern Spanish Pyrenees [*Rushlow et al.*, 2013]. The exact cause for late postorogenic exhumation is still debated, but the excavation of paleovalleys filled by Oligocene-Miocene conglomerates could account for the observed ages [*Fillon and van der Beek*, 2012]. The Ebro Basin was reconnected to the Mediterranean domain in the Tortonian at 10–7 Ma [*Garcia-Castellanos et al.*, 2003; *Urgeles et al.*, 2011; *Fillon and van der Beek*, 2012; *Fillon et al.*, 2013], although a connection during the Messinian [*Coney et al.*, 1996] or after [*Babault et al.*, 2006] has been proposed.

2.2.3. North Pyrenean Zone and Aquitaine Foreland Basin

The northern Pyrenean fold-and-thrust belt constitutes the retrowedge of the Pyrenees (Figures 1 and 5). It is divided into the North Pyrenean Zone (NPZ) and the Sub-Pyrenean domain, separated by the North Pyrenean Frontal Thrust (NPFT). The NPZ consists of variably metamorphosed Mesozoic "black flysch" of Albian age, some of them involving penetrative Alpine cleavages, and Paleozoic crystalline basement (Figure 5). The northern Pyrenean crystalline massif is interpreted as the basement of Albian half-grabens reactivated and inverted during the Late Cretaceous [*Desegaulx et al.*, 1990].

The Pyrenean HT-low-pressure metamorphism characterizes a narrow band of 10 km. This metamorphism lasted almost 25 Ma between 110 and 85 Ma [*Albarède and Michard-Vitrac*, 1978; *Montigny et al*., 1986] and was associated with Albo-Cenomanian K volcanism [*Montigny et al*., 1986] and crustal thinning [*Golberg and Leyreloup*, 1990]. In the central Pyrenees, magmatism is 110–100 Ma and metamorphism appears slightly younger 93–95 Ma. Temperature estimates along the NPF reach 500°C in the Jurassic-Cretaceous pelitic assemblage [*Golberg and Leyreloup*, 1990], 340–390°C in the mylonitic limestones in the eastern Pyrenees [*Vauchez et al*., 2013], increasing to 600°C in the Aulus Basin. Overall, the RSCM (Raman Spectrometry on Carbonaceous Material) data indicate decreasing temperature from east to west in the northern Pyrenees [*Clerc and Lagabrielle*, 2014]. Both metamorphism and magmatism appear temporally and geographically associated with the occurrence of peridotites (lherzolites) or middle-to-lower crustal materials, suggesting a genetic link with extension and mantle exhumation [*Vielzeuf and Kornprobst*, 1984; *Lagabrielle and Bodinier*, 2008; *Jammes et al*., 2009; *Lagabrielle et al*., 2010; *Clerc et al*., 2012; *Clerc and Lagabrielle*, 2014].

Mylonitic deformation is dated at 110–100 Ma [*Costa and Maluski*, 1988] across extensional shear bands and is associated with HT metamorphism as reported in the Variscan gneiss of Saint Barthelemy [*Passchier*, 1984; *de Saint-Blanquat et al*., 1990; *Vauchez et al*., 2013]. The extension is found associated with talc-chlorite mineralization dated at 112–97 Ma [*Schärer et al*., 1999] and granite albitization at 117 Ma [*Boulvais et al*., 2007] suggesting a single tectonic-hydrothermal event. There are synkinematic mineral assemblages in ductile shear zones that indicate top-to-the north stretching associated with extension under HT conditions [*Golberg and Leyreloup*, 1990; *Vauchez et al*., 2013]. In addition, stretching lineations associated with the metamorphosed and folded sediments support North-South shortening under HT conditions [*Choukroune*, 1974]. However, the age of HT deformation is not well constrained.

To summarize, both tectonic and sedimentary processes can be accounted for by hyperextension and exhumation of the subcontinental mantle during the Aptian-Albian [*Lagabrielle and Bodinier*, 2008; *Jammes et al*., 2009; *Lagabrielle et al*., 2010]. In this context, part of the exhumation of middle to lower crustal rocks found in the northern Pyrenees (e.g., granulite) can be linked to the Aptian-Albian extension.

The Coniacian-Santonian (88–83 Ma) marks a period of transition in the NPZ as the foreland basin developed in a transpressional context [*Déramond et al*., 1993] (Foix geological map). Turbiditic sandstones of this age were deposited in association with mass and debris flows and contain Paleozoic clasts supplied from the south. As Figure 6 shows, the synrift series composed of Lower Cretaceous flyschs and breccias are thrusted along the NPFT on top of synorogenic Late Cretaceous and Paleogene wedge-top deposits of the Sub-Pyrenean domain. In the Aquitaine Basin the foreland subsidence shifted toward the north and became more important at the Cretaceous-Paleocene transition ~65 Ma [*Desegaulx et al*., 1990, 1991]. Danian series overlapped on the NPFT along the western continuation of the Pech de Foix structure, showing that at least part of NPFT movement ceased by this period (Figure 6) [*Desegaulx et al*., 1990]. The Late Cretaceous flysch basin was topped by early Paleocene continental deposits and marine Ypresian series. From late Ypresian to Mio-Pliocene, the Aquitaine retroforeland basin was filled with up to 4700 m of alluvial and fluvial deposits (e.g., Oligocene to Miocene Molasses of the Palassou Formation and Lannemezan Formation) [*Plaziat*, 1981; *Biteau et al*., 2006].

Few bedrock ZFT ages reported in the northern Pyrenees Massifs suggest that synconvergence cooling initiated as early as 70 Ma [*Whitchurch et al*., 2011]. AFT ages in the Lacourt Massif and in the western part of the Arize Massif (Figure 5) yielded ages ranging between 55 and 37 Ma with a break-in slope in the age-elevation profile that suggests an acceleration at about 50 Ma [*Fitzgerald et al*., 1999]. However, as pointed out by *Sinclair et al*. [2005], these data could fit equally well another scenario in which exhumation was slow and steady after 50 Ma and accelerated only after 38 Ma.

The timing of deformation in the Sub-Pyrenean domains, including folding in the Lavelanet and Mas d'Azil anticline, is provided by the observation of a sharp decrease in bedding dips within the Palassou Formation of early Oligocene (lower Rupelian) age ~33 Ma (Figure 6). These formations are overlain by late early Rupelian deposits, which are slightly inclined toward the north. This indicates that frontal accretion in the northern Pyrenees ceased before 28 Ma, in agreement with the sharp decrease of North-South shortening amount after 30 Ma observed in the foreland of the western Pyrenees [*Rocher et al*., 2000].

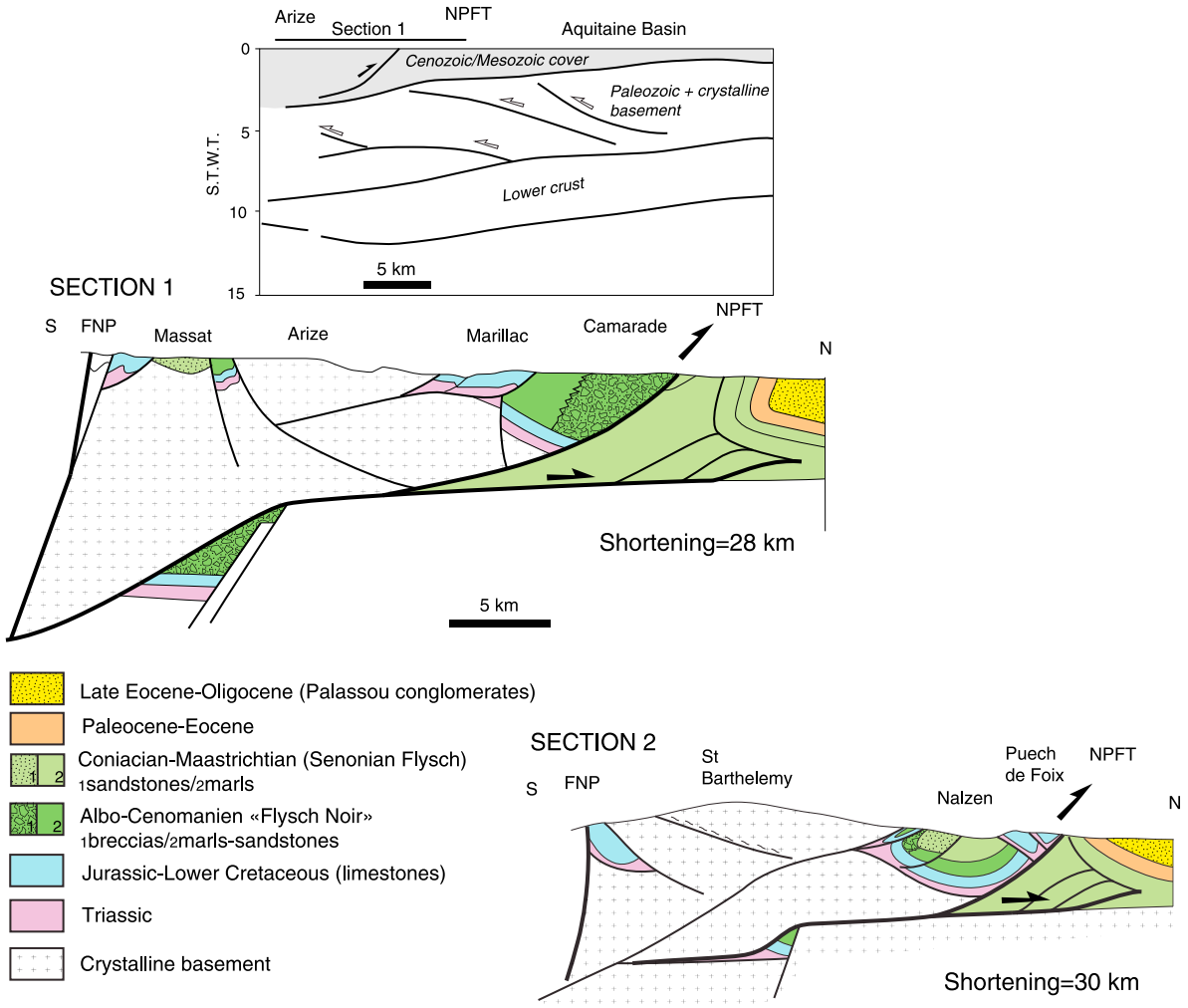

Figure 6. Geological balanced sections across the northern Pyrenees redrawn after *Baby* [1988] (location in Figure 5) and line drawing from interpretation of the ECORS profile parallel to section 1 [*Choukroune et al*., 1990] showing the north facing Variscan thrusts negatively inverted during the Permian. The sections outline an overall thick-skinned style with prominent basement-involved shortening. According to the interpretation of the ECORS profile [*Baby*, 1988; *Roure et al*., 1989; *Muñoz*, 1992], the NPFT is a low-angle, south dipping, crustal thrust ramp rooting into the layered lower crust or the mantle.

3. Geochronological and Low-Temperature Thermochronological Constraints in the Northern Pyrenees

3.1. Sampling in the Northern Pyrenees and Analytical Methods

To improve our understanding of the early stages of compressional deformation and to bridge the gap with tectonostratigraphic datasets in the northern Pyrenees, we have carried out a detrital study combining U/Pb, ZHe, and AFT dating. Three sandstone samples have been collected in Paleocene to early Eocene synorogenic deposits of the northern Pyrenees, in the footwall of the NPFT (Figure 7).

The oldest sandstones were sampled in the northern limb of Roquefixade anticline (Figure 7a). They correspond to Paleocene meandering fluvial sandstones of the Auzas Marls Formation, deposited in a semiarid floodplain environment (RAP1; circa 65 Ma). These sediments are stratigraphically equivalent to the upper Garumnian red beds dated to the Maastrichtian-Paleocene boundary in the SPZ [*Plaziat*, 1981; *Ardèvol et al*., 2000; *Schmitz and Pujalte*, 2007]. Paleogeographic reconstructions suggest that these sandstones were sourced from the rising Axial Zone in the east [*Plaziat*, 1981]. In the southern Aquitaine Basin, the Auzas Marls Formation overlies the Maastrichtian Labarre fluvial sandstones, which are covered by the Thanetian Milliolid Limestones.

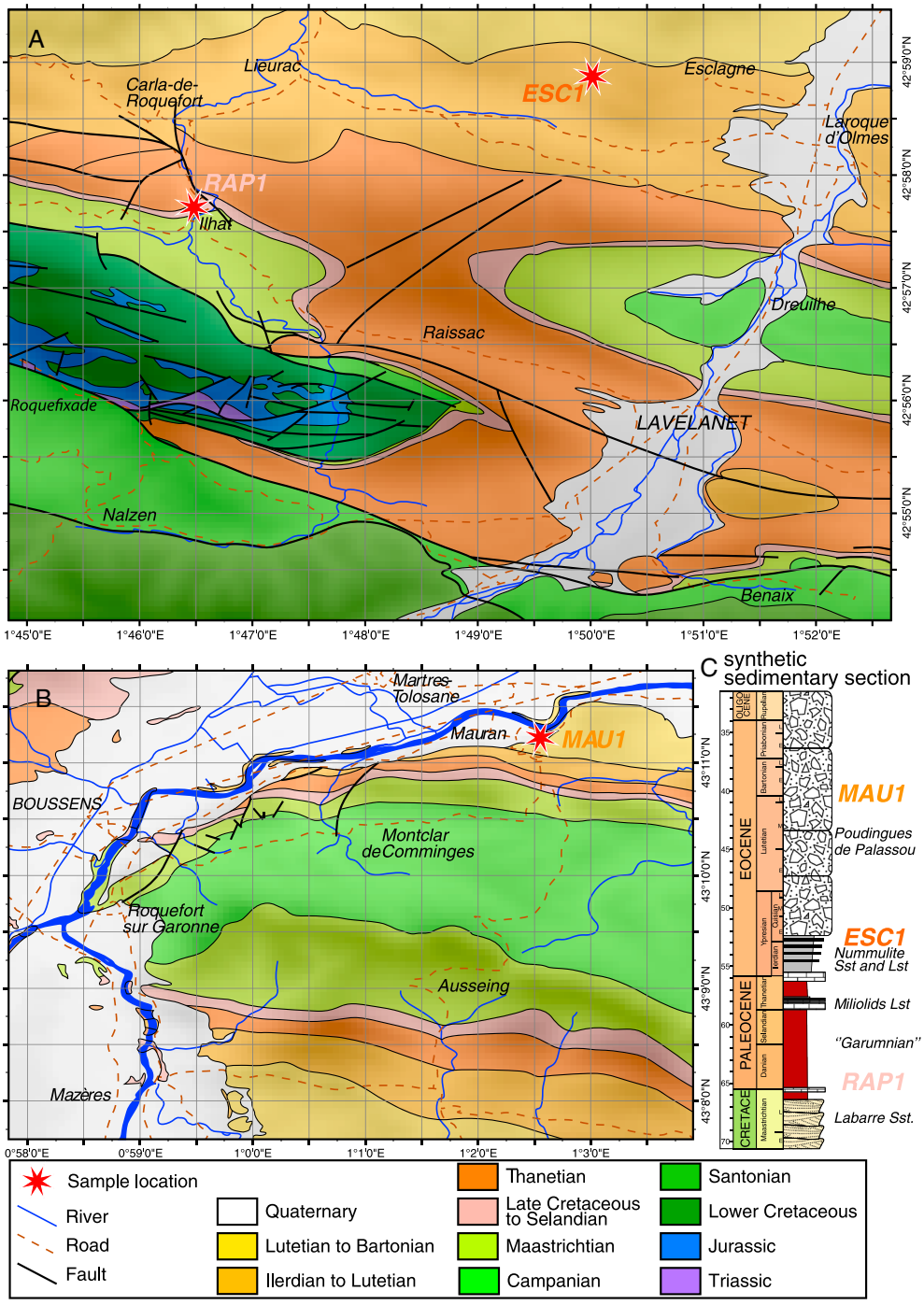

Figure 7. Sampling sites for U/Pb, ZHe, and AFT analyses in the northern Pyrenees (location of maps in Figure 1). Samples RAP1, ESC1, and MAU1 are replaced on a generic lithostratigraphic section.

The second sample (ESC1) was collected in the northern limb of Lavelanet anticline (Figure 7a), above the last marine deposits of the North Pyrenean basins (Nummulite Limestones). The ESC1 sandstones were sampled in the "Couches de Léran" coarse distal sandstones interbedded with floodplain marls. They are dated to Ypresian (circa 52–53 Ma). This formation is the first member of the Poudingues de Palassou Formation (Ypresian to Oligo-Miocene). The sedimentary sources are also located in the Axial Zone to the south [*Plaziat*, 1981].

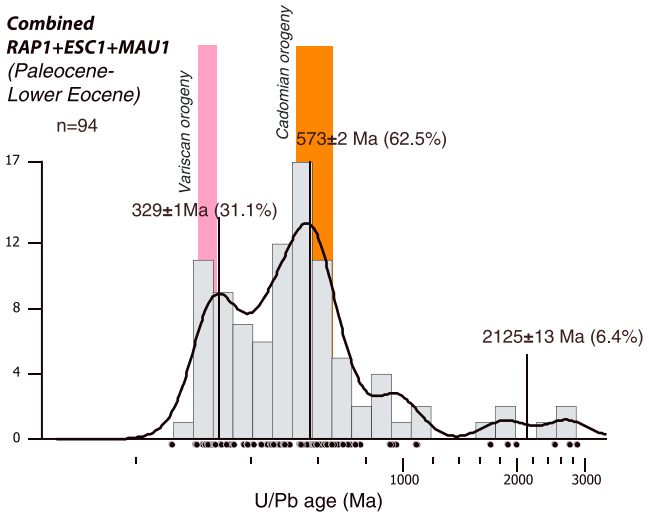

Figure 8. Detrital age distribution of zircon U-Pb ages for Cenozoic strata in the southern Aquitaine Basin (early Paleogene, RAP1; middle Eocene, ESC1; late Eocene, MAU1). Both histograms in 20 Ma bins and age probability plots are shown.

The third sandstone sample was collected in the Palassou Conglomerate Formation (Figure 7b), in coarse-grained sandstones interbedded within conglomerates (MAU1; circa 40 Ma).

3.1.1. Zircon U-Pb Geochronology

A total of 94 zircon grains were selected randomly from the 50 to 500 μm fraction of the three studied samples, mounted in the epoxy resin, and slightly polished (about 20 μm). The U/Pb ages were determined by in situ secondary ion mass spectrometry (SIMS) analysis (Centre de Recherches Pétrographiques et Géochimiques's CAMECAIMS1270) following the approach described in *Deloule et al.* [2002], using results from the 91,500 standard dated at 1,062.4 ± 0.4 Ma [*Wiedenbeck et al.*, 1995]. Photographic maps were produced for each sample to locate the same grains for subsequent retrieval and (U-Th)/He analysis. The spot size of the ion microprobe varied between 30 × 40 and 40 × 50 μm, with the beam positioned in the center of each grain. As the measured zircons were generally larger than 100 μm in diameter, we consider that the measured ages do not represent a mean of the various potential age zonations in case of complicated metamorphic history but rather the age of the oldest thermal event that affected the grain. Correction for common lead was made using the amount of ^{204}Pb and applied to the ^{207}Pb/^{206}Pb age following the model of *Stacey and Kramers* [1975].

3.1.2. Zircon (U-Th)/He Thermochronometry

Among the 94 zircon grains, we have selected 31 zircons for (U-Th)/He thermochronometry on samples ESC1 and MAU1. These were chosen so as to represent the main peaks individualized in the U/Pb age distributions. Zircon grains from the previously U/Pb-dated populations were retrieved from the SIMS mounts, loaded in Pt capsules, outgassed at 1300°C for 20 min, and analyzed for He concentrations with a VG603 noble gas mass spectrometer [*Pik et al.*, 2003]. The U and Th were measured (based on reference materials) with accuracy and reproducibility of 2–3% during this period of analysis. Total procedure blanks were generally less than 2% (maximum 5%) of the U and Th concentrations in the solution. The overall precision of He ages determined with this procedure is approximately 8% (2σ). Zircon ages were calculated and corrected for α emission following the procedure of for pyramidal tetragonal prisms [*Ketcham et al.*, 2011]. Abrasion prior to running the samples has been restricted to about 25% of the grains, to limit the amplitude of additional uncertainties during Ft correction.

3.1.3. Apatite Fission Track Thermochronology

Samples were prepared for AFT analysis at ETH Zurich. Apatite grains were separated from approximately 5 kg bulk samples using standard heavy liquids and magnetic separation techniques. Spontaneous tracks were revealed through polishing of grain mounts and etching with 5.5 N HNO_3 at 21°C for 20 s. Samples were irradiated with thermal neutrons at the Oregon State University Triga reactor (USA) with a nominal neutron fluence of 1E16 n cm^{-2}. The standard glass CN-5 was used as a dosimeter to measure the neutron fluence. After irradiation, induced fission tracks in the external detectors (low-U muscovite) were etched in 40% HF at 21°C for 40 min. Apatite fission track central ages (±1σ) [*Galbraith and Laslett*, 1993] were measured and calculated using the zeta calibration methods with International Union of Geological Sciences age standards [*Hurford and Green*, 1983]. In case of nonreset detrital samples, showing multiple source rocks with different cooling ages or varying exhumation rates, we have decomposed grain age distributions using the kernel distribution estimation (KDE) peak-fitting method [*Vermeesch*, 2009, 2012]. To bring better constraints on both predepositional and postdepositional thermal histories of our samples, we modeled our AFT data using QTQt [*Gallagher et al.*, 2009; *Gallagher*, 2012] taking into account the most recent multikinetic AFT annealing

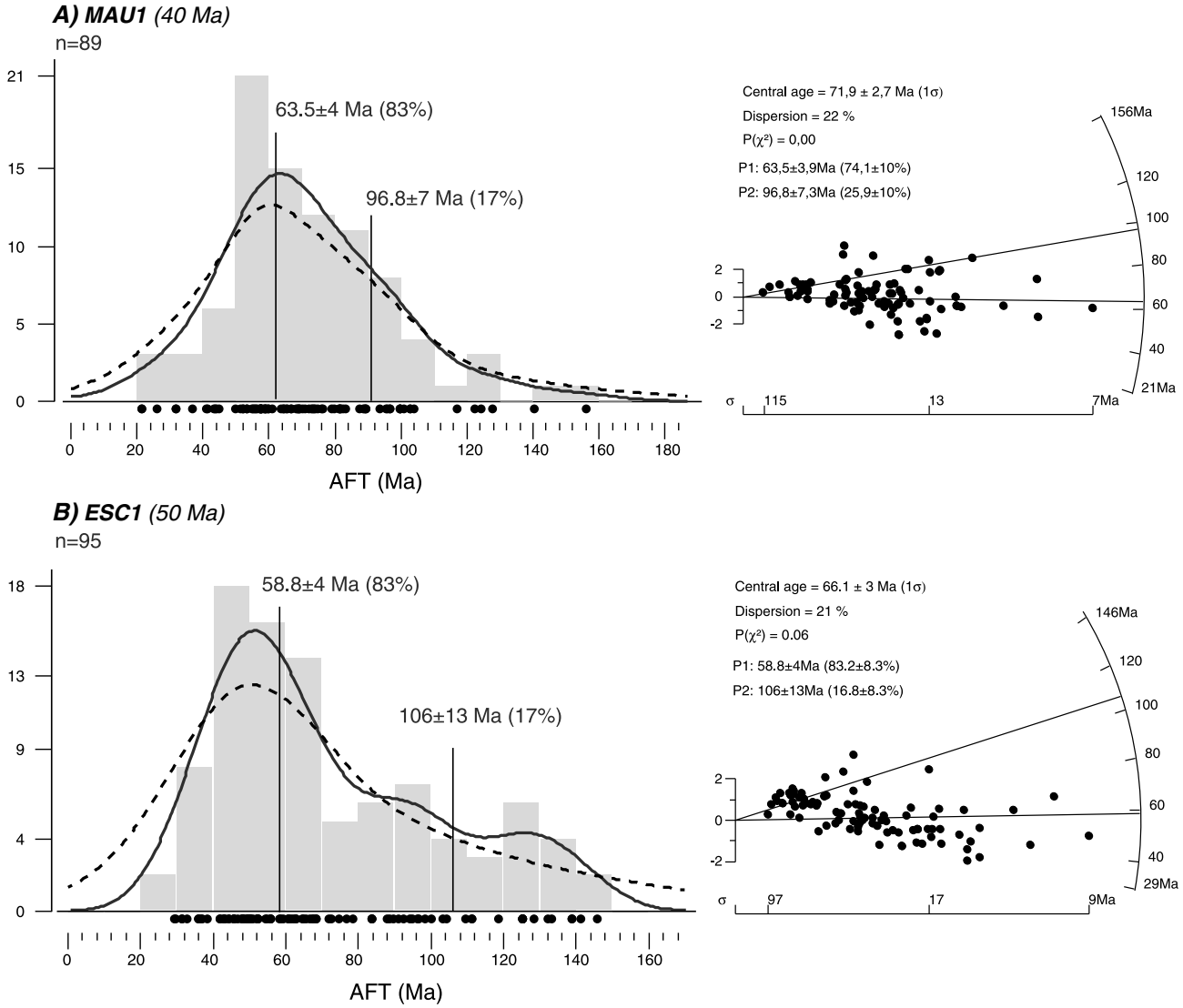

Figure 9. AFT age distribution for (a) 89 counted grains in MAU1 sample and (b) 95 counted grains in ESC1 sample. For each sample, the black curve represents the probability density plots with associated error as a grey envelop. This is derived from histogram representations using RadialPlotter program [*Vermeesch*, 2009].

model of [*Ketcham et al.*, 2007]. The inversion procedure allows us to determine the best time-temperature path reproducing our data through a large number (>200,000) of randomly tested solutions. Details of the modeling procedure are given by *Gallagher* [2012].

3.2. Results

3.2.1. Zircon U-Pb Age Data

Results of the 94 U/Pb analyses are reported in Table S1 in the supporting information. Because the number of U/Pb-dated zircons per sample is below the number of zircons per detrital sample, theoretically needed in provenance studies [*Vermeesch*, 2004], we only discuss age peaks for combined samples (Figure 8).

All samples present similar U/Pb age peaks, although their proportions are variable (Figure 8). When combined, two main populations are observed. The first age peak is Cambrian (573 ± 2 Ma, 62.5%) and the second is represented by Variscan zircon grains (329 ± 1 Ma, 31.1%). A third subordinate population shows grains with Paleo-Proterozoic age (2125 ± 13 Ma, 6.4%).

3.2.2. Apatite Fission Track Thermochronology and Inverse Modeling

In the ESC1 sample, 95 grains were counted, and they give a range of ages between 30 and 147 Ma that can be separated into two populations by KDE peak fitting (Figure 9 and Table 1). The youngest population P1 is

Table 1. Detrital Apatite Fission Track Analytical Data[a]

Sample	Latitude (°N)	Longitude (°N)	No. of Grains	N_d	ρ_d (Tracks/cm^{-2})	N_s	ρ_s (Tracks/cm^{-2})	N_i	ρ_i (Tracks/cm^{-2})	$P(\chi)^2$ (%)	Disp. (%)	Grain Age Range (Ma)	P1 (Ma)	P2 (Ma)
ESC1	42.981367	1.83675	95	4739	1.52E+06	948	1.63E+06	3619	6.21E+06	5.9	21	30–147	58.8 ± 4 (83%)	106 ± 13 (17%)
MAU1	43.19225	1.039733	90	5637	1.81E+06	1951	2.13E+06	9402	1.03E+07	0.7	17	21–131	63 ± 4 (74%)	96 ± 7 (26%)

[a]No. of grains: total number of counted grains; N_d and ρ_d: total number and density of induced tracks on dosimeter; N_s and ρ_s: total number and density of spontaneous tracks; N_i and ρ_i: total number and density of induced tracks on samples. All samples were counted by Pierre-Yves Filleaudeau using a zeta of 332.46 ± 13.48. Calibration factor, ζ, has been determined by using CN-5 glass standard. $P(\chi^2)$ is chi-squared probability that grain ages are concordant, and Disp. is the grain age dispersion. A sample may contains multiple age populations if $P(\chi^2) < 5$ and/or Disp. > 15 [*Galbraith and Green*, 1990; *Galbraith and Laslett*, 1993]. P1 and P2 are age populations calculated using the KDE peak fitting and are given ±1σ. Also given is the percentage of grains in a specific peak.

Paleocene (58.8 ± 4 Ma, 83%) and therefore displays a synorogenic signature. The oldest, and less well-resolved, population P2 is Albian (106 ± 13 Ma, 17%). Eighty-nine grains were measured in MAU1 sample, showing single-grain ages scattered between 21 and 131 Ma. Two age peaks are also identified. The youngest synorogenic population P1 is Late Cretaceous-Paleocene (63 ± 4 Ma, 74%). The oldest population P2 recognized in MAU1 is Cenomanian (96 ± 7, 26% of grains). Although our age populations are older than the depositional ages for both samples, a non-negligible proportion of the grains are younger. This is most obvious for the oldest, and more deeply buried ESC1 sample, where 10-15 single grain ages overlap with the depositional age (~50 Ma) or are younger. The scattering of detrital AFT ages in ESC1 and MAU1 suggests different sources and pre-depositional thermal histories. To test the possible effect of reheating in the Pyrenean foreland and define a consistent thermal history for both samples we conducted an inverse modeling approach using QTQt [e.g. *Gallagher*, 2012].

In our inverse model of the detrital AFT ages, we assumed that the dated grains belong to either one of the populations defined by the peak-fitting (Esc1-P1/Esc1-P2 and Mau1-P1/Mau1-P2). In order to resolve the syn-collisional evolution, we focus on the modeling of the youngest populations P1, which is treated as one sample with 79 and 66 grains for ESC1 and MAU1, respectively (Figure 10). Reset grains are included to gain constraints on postdepositional burial. The inversion procedure assumes that each grain within each sample "P1" (ESC1-P1 and MAU1-P1) shared the same predepositional cooling history. Despite bias inherent to the analysis of detrital data, this approach returns probabilities from which the most statistically representative time-temperature history for P1 populations is deduced. As such it is intended to define cooling rates better than a more direct lag time approach.

The diameter of the track etch pits (D_{par}) was not measured. Therefore, to examine the effect of different AFT kinetic parameters on the levels of annealing, we used in the modeling different average low (1.5 μm) and high (2.5 μm) *D*par values. We also tested the impact of the youngest grains on the model solutions. These tests emphasize that modifying the annealing properties of the grains or adding young grains only slightly affect the model results. The inversion starts from 200 Ma and includes time-temperature constraints for deposition at 50 ± 5 Ma (ESC1) or 40 ± 5 (MAU1), with a temperature of 10 ± 5°C (surface conditions). We run 200,000 simulations, a number high enough to obtain a stable and robust solution (see discussion by *Gallagher* [2012]). The results are presented in Figure 10.

The models show very similar time-temperature paths for both samples. Postdepositional heating for populations P1 appears limited (10–35°C) suggesting maximum burial in the foreland basin of less than 1.15 km at 30–20 Ma, assuming a geothermal gradient of maximum 30°C/km. Cooling resumed after 20 Ma. The P1 models allow to resolve a predepositional cooling from 70–75 Ma and temperatures of maximum 110°C. These results indicate a cooling rate of about 5.5°C/Ma (exhumation rates of 0.18 km/Ma for a geotherm of 30°C/km). For comparison, a lag time approach would have resulted in higher cooling rates ranging between 6°C/Ma (MAU1) and 12°C/Ma (ESC1).

3.2.3. Zircon (U-Th)/He Age

ZHe analyses were performed also on samples ESC1 and MAU1 (Figure 11 and Table S2 in the supporting information). Single-zircon grain ages show a scatter of age ranging from 51 ± 4 Ma to 390 ± 31 Ma for ESC1

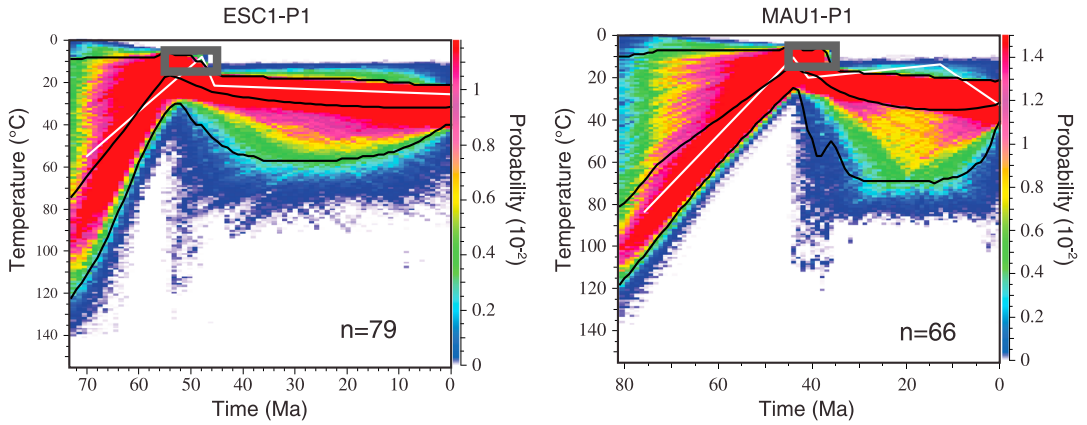

Figure 10. Time-temperature paths defined from inverse modeling of AFT data for grains of populations P1 in samples ESC1 and MAU1 (see also Figure 9). Colors refer to the probability of a model time-temperature path to be resolved at a given time-temperature point (scale in the right side varies for each model). The grey boxes represent time-temperature constraint adopted in the modeling that is the depositional age. The different timescales are constrained by the oldest single-grain AFT age modeled. Number shows the amount of individual grain per population P1 in each sample. The black lines represent the expected models (the weighted mean model and its 95% confidence interval), and the white line is the maximum likelihood model that corresponds to the best data fit.

($n = 17$) and from 48 ± 4 Ma to 276 ± 22 Ma for MAU1 ($n = 14$). Given the uncertainties on depositional ages, ZHe data suggest a possible partial postdepositional resetting for ESC1 (depositional age of 50 ± 5 Ma). However, the time-temperature history deduced from AFT data (Figure 11) indicates maximum burial temperatures far below the closure temperature of the ZHe system. We therefore infer that ZHe data are not reset. In order to gain maximum resolution on grain age peak fitting, samples ESC1 and MAU1 were combined. This is acceptable due to the 10 Ma time span between samples and ±5 Ma stratigraphic resolution on depositional ages as well as the consistent age distribution between samples. The combined 31 (U-Th)/He grain ages of ESC1 And MAU1 are reported and plotted on the age density diagram of Figure 11, which also shows the four age components recovered by peak fitting analyses. One dominant peak is Santonian (82 ± 2 Ma; 50.3%). Two equally represented populations are Paleocene (53 ± 2 Ma; 20.7%) and Lower Jurassic (176 ± 5 Ma; 19.4%). A poorly resolved age peak is Permian at 285 ± 14 Ma (10%). The Paleogene population indicates lag times lower than ~10 Myr, similar to those based on the AFT data. Nevertheless, given the uncertainly of the depositional age, inferring an exhumation rate would be speculative. The 82 Ma age peak is represented by a group of zircon grains ranging between 80 Ma and 105 Ma that overlap the age of the onset of convergence. The occurrence of preorogenic and synorogenic populations with long lag times (30–50 Myr) in the same paleodrainage area suggests that during the Pyrenean orogenesis the source rocks of the dated zircons recorded a low thermal overprint (close to the ZHe closure temperature ~180°C) that caused only either partial or local resetting.

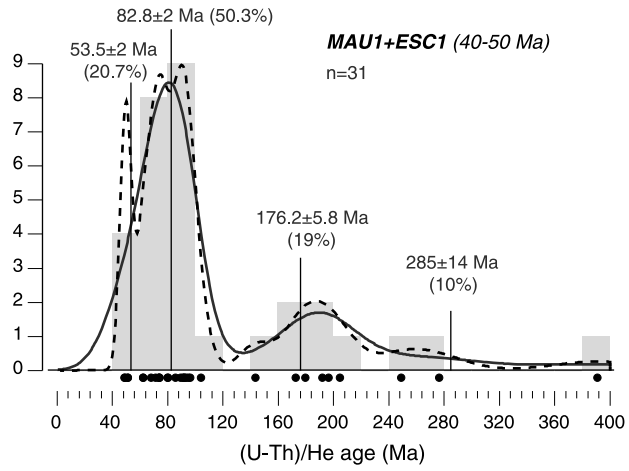

Figure 11. Detrital zircon (U-Th)/He ages for Cenozoic strata in the southern Aquitaine Basin (middle Eocene, ESC1; late Eocene, MAU1). Both histograms in 20 Ma bins and age probability plots are shown.

3.3. Cooling/Exhumation Patterns in the Northern Pyrenees: From Rifting To Orogeny

The distribution of the detrital U/Pb ages (Figure 8) is characterized by predominant Cambrian ages associated with the Cadomian orogeny, subordinate Late Paleozoic ages related to the Variscan orogeny and rare Paleoproterozoic-Archean grains of the pre-Cadomian basement. A similar U/Pb age distribution has been recognized in the southern Pyrenees from Maastrichtian sediments [*Whitchurch et al.*, 2011]. We interpret the Variscan ages as related to first-cycle

zircons eroded from granitic bodies. Cadomian grains reflect the U/Pb signature of magmatic, and volcano-clastic rocks now exposed in the eastern Pyrenean Axial Zone and the North Pyrenean Zone [*Deloule et al*., 2002; *Laumonier et al*., 2004; *Castiñeiras et al*., 2008; *Denèle et al*., 2009]. Alternatively, they can be recycled zircon preserved in Ordovician orthogneisses exposed in the Arize, Trois Seigneurs, Aston, and Hospitalet Massifs or from Cadomian rocks outcropping in the eastern Pyrenees. We ascribe the rare Proterozoic grains as inherited and recycled from ancient continental crystalline pre-Cadomian basement not observed in the Pyrenees.

In addition to the similarities in the U/Pb detrital record between the northern and southern Pyrenees, our detrital ZHe ages show a Late Triassic to Early Jurassic population similar to one recovered in older Late Cretaceous samples of the southern Pyrenees [*Filleaudeau et al*., 2011]. This can be correlated with the widespread ophitic magmatism and more generally with a major magmatic episode associated with the central Atlantic Magmatic Province [*Marzoli et al*., 1999] at circa 200 Ma.

While age populations older than 150 Ma are retained only by the ZHe and U/Pb systems, two age populations in the ranges of 80–105 Ma and 50–65 Ma, respectively, are found in both the AFT and ZHe distributions (Figures 9 and 11). A ZFT population in the range 95–111 Ma was reported also in the southern Pyrenees [*Whitchurch et al*., 2011]. Thus, thermochronometric signatures at ~100 Ma recur in the southern and northern Pyrenees and in three dating systems. These signatures can be related to cooling after the maximum crustal thinning in the Albian, when peak temperatures related to crustal breakup were reached. The signature at 50–65 Ma records an early synorogenic stage of cooling. Our inverse modeling of AFT data allows resolving the onset of the synorogenic, in the northern Pyrenees, back to 70–75 Ma and exhumation of ~0.2 km/Myr until 40–50 Ma (Figure 10). These rates are in good agreement with other estimates from southern Pyrenees circa 70–60 Ma [*Beamud et al*., 2011].

Other bedrock fission track data in the Lacourt Massif complement these results by showing accelerated thrust-related exhumation at similar rate of 0.2 km/Myr from 50 Ma to 36 Ma [*Fitzgerald et al*., 1999]. Finally, our samples experienced burial in a foreland basin before final postorogenic exhumation after 20 Ma (Figure 10).

The wide age range (40 to 400 Ma) of our ZHe data as opposed to the absence of ages older than 150 Ma in our AFT record may be interpreted as indicative of cooling and exhumation from very shallow crustal levels, assuming that apatites and zircons came from the same source rocks. This interpretation fits well with an early synorogenic scenario when deeply exhumed rocks are unlikely to have yet been exposed.

4. Limits to Shortening Magnitude in the Central Pyrenees From Balanced Cross Sections and Thermal History

4.1. Northern Pyrenees

Figure 5 presents the main geological features of the northern central Pyrenees. Two balanced cross sections available in the region [*Baby*, 1988] suggest deformation is the result of the reactivation and inversion of Albo-Cenomanian extensional basins and its crystalline basement (Figure 6). They reveal shortening magnitude of 28–30 km, mostly accommodated by thrusting in the hanging wall of south dipping NPFT. This main thrust is imaged on the wide-angle ECORS seismic profile [*Roure et al*., 1989] and is seen to connect with an anomalous positive gravity anomaly below the 3S Massif. These values represent minimum shortening. First, because footwall cutoff is determined from the position of the lower Cretaceous, which is not constrained by subsurface data, a minimum distance is therefore assumed based on the restored length of upper Cretaceous (Senonian) foreland strata. Second, the exact position of the Albo-Cenomanian basin before tectonic inversion is unknown. It is largely dependent on the extensional movements assumed on the faults bordering the 3S and Arize Massifs. For instance, the presence of north facing Variscan thrusts reactivated during Permian extension (see line drawing of Figure 6; see also *Choukroune et al*. [1990] or *Roure and Choukroune* [1998]) are not taken into account in the interpretation shown in section 1. Moreover, this estimate does not include mesoscale folds and faults nor a component of ductile shortening that could locally account for up to 50% [*Choukroune*, 1974].

The determination of shortening magnitude in the region of Lherz (Aulus Basin) is not straightforward because both the kinematics of deformation and exact internal structure of the basin are not well constrained, despite recent attempts [*Clerc et al*., 2012]. The positions of hanging wall cutoffs that limit the

Aulus Basin are unknown due to erosion. Finally, the Aulus Basin is located in the suture zone and cannot, alone, inform us on the total shortening absorbed in this domain due to the lack of continuous stratigraphic markers and loss of material in subduction. Searching for a genetic link between this feature and a mechanism responsible for mantle exhumation in Lherz suggests that the NPFT inverted a low-angle detachment system cutting the whole crust down to the mantle [*Lagabrielle et al*., 2010]. This reveals that a significant part of the total convergence was partitioned in the region of Lherz but cannot be estimated from classical balancing techniques alone.

Low-temperature thermochronological data can be helpful here to distinguish between different crustal fragments that recorded variable thinning, and subsequent cooling during thermal relaxation and exhumation. Deformation in the distal margin, located in the Aulus Basin likely started after convergence initiation at 83 Ma. Widespread East-West cleavages in the Mesozoic cover, close to the NPF, argue for ductile shortening at shallow crustal level. Preliminary results, in the western Pyrenees, reveal that the residual high geothermal gradient inherited from the Albo-Cenomanian extension may last up to 30 Myr after convergence onset [*Vacherat et al*., 2014]. This process may explain compressional ductile deformation recorded in this region without significant tectonic burial. Cooling recorded at 75–70 Ma from our AFT data (Figure 10) likely correlates with onset of thrust-related exhumation. From this time until 36 Ma, erosion and mountain building led to foreland deposition in the Aquitaine Basin. Syntectonic deposition in the Sub-Pyrenean Zone reveals that NPFT movement lasted until 28 Ma. A shortening of 28–30 km estimated from sections of Figure 6 reflects a minimum amount because it does not account for convergence absorbed in the suture region, i.e., the distal hyperextended margin.

4.2. Southern Thrust Belt

The southern Pyrenees is by far the most documented part of the orogen, thanks to numerous good quality wells and seismic and outcrop conditions, allowing tectonostratigraphic relationships to be well constrained. Most data and structural interpretations are presented in *Vergés* [1993]. A cross section of the southern Pyrenees (Figure 3) shows division of the thrust belts into the Sierras Marginales, Montsec, and Bóixols thrust sheets [*Muñoz*, 1992; *Beaumont et al*., 2000]. The main component of shortening is taken up by a main thrust ramp that carries Triassic rocks on top of Eocene rocks south of the Sierras Marginales and Montsec units. The magnitude of shortening is constrained from the position of the footwall cutoff. It is first defined by Comiols-1 and Isona-1 wells [*Lanaja*, 1987; *Vergés*, 1993; *Filleaudeau*, 2011] where the Triassic is seen to lie tectonically above the Eocene (Figure 12). The décollement in the Triassic may extend to the north, but it is limited by the position of the San Corneli-1 well, because the well shows no evidence for tertiary rocks below the Bóixols thrust ramp. A maximum North-South shortening value is obtained if we assume that the footwall of the Montsec thrust, as inferred from the position of the Eocene, terminates at the Bóixols thrust [*Beràstegui et al*., 1990; *Vergés and Muñoz*, 1990]. Following this interpretation (Model A, Figure 3), a post-Oligocene North-South shortening of 45 km is reconstructed, of which 29 km is accommodated by translation (no internal shortening) of the cover thrust sheets [*Meigs and Burbank*, 1997]. Overall, the total amount of shortening inferred is 165 km [*Beaumont et al*., 2000].

An alternative interpretation (Model B) of the same subsurface data [*Desegaulx et al*., 1990; *Choukroune*, 1992; *Meigs and Burbank*, 1997] relies on the importance given to Isona-1 for constraining North-South shortening. Isona-1 is located laterally to the ECORS section, in a region where tectonic transport occurred oblique to the North-South shortening, i.e., in the SE direction in association with the Segre oblique ramp (Figure 12). It is therefore possible that Isona-1 constrain the position of the footwall oblique ramp cutoff rather than North-South deformation along the ECORS section further to the west. If this hypothesis is correct, a much lower shortening value of 55 km is obtained for the southern Pyrenees. In this interpretation, deformation in the Axial Zone involves the stacking of the lower Iberian crust, in agreement with reconstruction from *Roure et al*. [1989].

These two interpretations provide lower and upper bounds of crustal shortening, which are necessary for evaluating existing plate kinematic reconstructions.

4.3. Stepwise Restoration

In this section we propose a stepwise restoration of a section that assumes minimum shortening in the southern Pyrenees (Model B) (Figure 13). Temporal constraints used in the reconstructions are from published

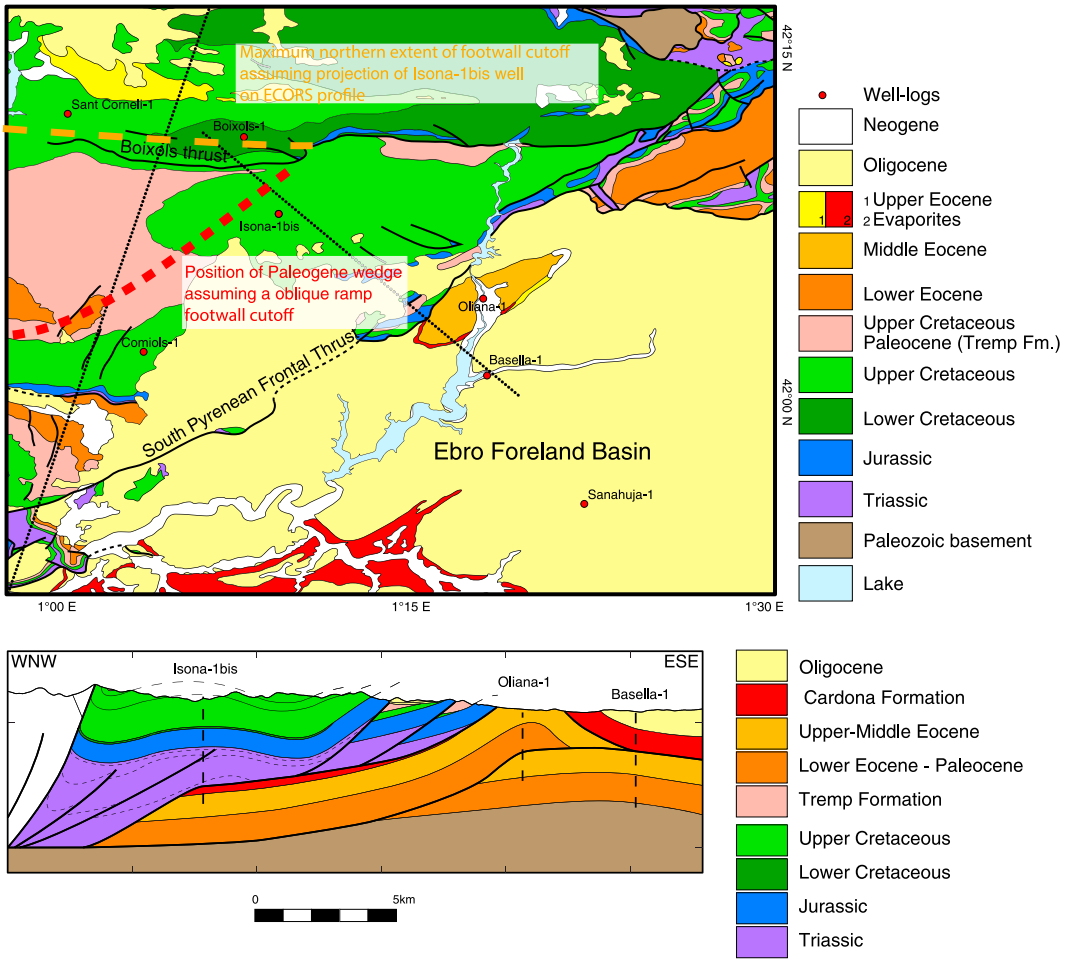

Figure 12. Position of possible footwall cutoffs below the main frontal detachment in the southern Pyrenees as constrained from available well data. Both scenarios define maximum and minimum estimates of shortening in the southern Pyrenees (see text for explanation). Below is a cross section across the Segre oblique thrust ramp.

tectonostratigraphic data and low-temperature constraints combined with our new low-temperature data. As recently exemplified in the Pyrenees, the use of quantitative interpretation of low-temperature data to assess a kinematic field inferred from balancing cross sections is far from being straightforward [*Erdős et al.*, 2014]. Poor resolution on topographic evolution from balanced cross sections and the impossibility to distinguish rapid versus slow cooling event due to the dependence on time intervals of the restoration, renders the solution at best nonunique. We therefore use these constraints with cautions. Our reconstruction accounts for recent *P* wave tomography and migration of converted *P* waves that revealed new details at the crustal and lithospheric scales (Figure 14) [*Chevrot et al.*, 2014a, 2014b]. *P* wave tomography data confirm results from resistivity measurements [*Campanyà et al.*, 2011] revealing an increase of the lithosphere thickness to ~130 km north of the NPF. This outlines the underthrusting of the Iberian lithosphere below the European lithosphere (Figures 13 and 14). A noticeable high *P* wave anomaly (blue) located at about 60 km below the northern Pyrenees appears to be well correlated with the northern extent of the Iberian Moho in contact with the European mantle. *Chevrot et al.* [2014b] interpret the interface between the top of the Iberian crust and the European mantle to be dipping 20° toward the north. In this region, the Iberian crust appears to be 10–20 km thick. This has been interpreted as the hyperextended Iberian margin subducted below the European mantle [*Chevrot et al.*, 2014b]. Alternatively, the thin Iberian crust could be only apparent and would simply result from the faulting of the Iberian crust, which was originally thicker. In our interpretation the contact between Iberian crust and European mantle is dipping 56° to the north but the difference is limited as seen on Figure 14. Taking into account the uncertainties on absolute velocities in this particular region, we suggest our structural solution remains valid.

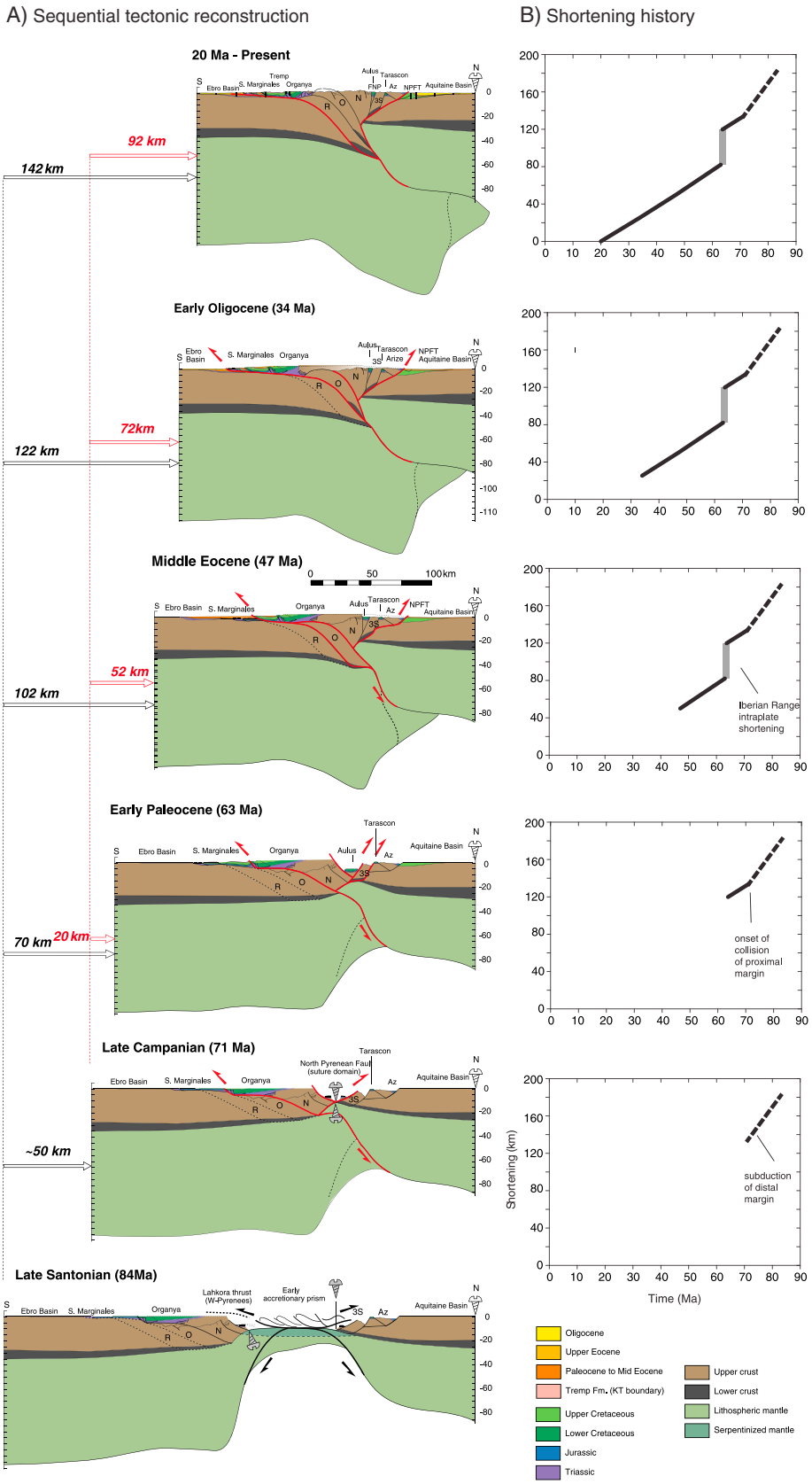

Figure 13

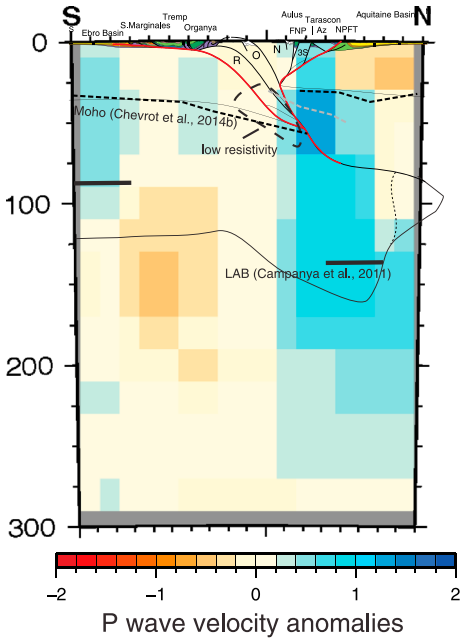

Figure 14. North-South vertical cross section of *P* wave tomography data projected along our cross section of Figure 13, in the central Pyrenees, after data obtained in *Chevrot et al.* [2014a]. Results from migration of converted *P* waves [*Chevrot et al.*, 2014b] outline the geometry of the Moho (black dashed lines) and the top of the Iberian crust (grey dashed line). Results from resistivity measurements [*Campanyà et al.*, 2011] are also shown. They reveal an increase of the lithosphere thickness to ~130 km north of the NPF (thick black horizontal lines).

Restorations have been obtained relative to the Cenomanian level, which is considered our preorogenic surface of reference. To account for the originally discontinuous synrift/prerift markers, we have considered variable thickness for pre-Cenomanian margin stratigraphic succession. The total shortening is reconstructed assuming a regional foreland pin line, which is the northern limit of the nondeformed European crust. In this reconstruction we assume crustal area and stratigraphic length conservation during shortening. In order to account for the upper lithospheric thickness in our reconstruction, we approximate the initial thickness of the mantle lithosphere prior to shortening using the approach of *Vergés et al.* [2011]. The thickness of the lithospheric mantle H_{lm} is given by $H_{lm} = \rho_{asth}\,(P_{wd} + H_0) - H_c\,(\rho_{asth} - \rho_{cr})/(\rho_{asth} - \rho_{mant})$ [*Lachenbruch and Morgan*, 1990] with H_c the thickness of the originally thinned crust for different margin sections, P_{wd} the paleobathymetry in rifted basins; H_0 is taken equal to 2.4 km and expresses the height of the sea level relative to the asthenosphere free surface; ρ_{asth}, ρ_{mant}, and ρ_{cr} are the asthenosphere density, mantle lithosphere, and crust densities. Details of the results are summarized in Table 2. Four exploration wells have been used (available on request to Bureau Exploration-Production des Hydrocarbures, http://www.beph.net) to constrain the geometry of the northern Pyrenees (Muret, Lezat, Pailhes, and Mas d'Azil). Five wells in the southern Pyrenees (Lerida, Guisona, Comiols, San Corneli, and Boíxols), most of them, are published in *Lanaja* [1987].

4.3.1. Early Oligocene-Miocene (34–20 Ma): Transition Toward Cessation of Collision

In the SPZ, a late stage of deformation between 37 Ma and ~25 Ma involved thrusting in the Sierras Marginales [*Meigs et al.*, 1996] and out-of-sequence movement along the Morreres back thrust (Figure 13). In the Axial Zone, exhumation is recorded in the Orri unit then Rialp unit [*Beamud et al.*, 2011]. The shortening magnitude estimated in the Sierras Marginales is approximately 15 km between 36.5 and 24.7 Ma [*Meigs et al.*, 1996]. Within the time interval studied, the situation shown in Figure 13 corresponds to the 29.5 Ma stage when the Sierras Marginales propagated to the south. The significant passive translation of southern thrust sheets between 36 and 30 Ma characteristics of Model A is therefore not shown here. Late deformation on the southern border of the Axial Zone appears coeval with increasing exhumation rates in the Orri unit up to 2–4 km/Myr during the period ranging from 35 to 32–30 Ma, followed by a sharp reduction until 20 Ma [*Fitzgerald et al.*, 1999]. The cause of this relatively short-lived period of rapid exhumation is unclear. Focused exhumation in the south may have triggered accrued deformation by internal shortening of the orogenic wedge, through thrust reactivation of existing thrusts or folding. Because most thrust units were already

Figure 13. Sequential restoration of central Pyrenees from 83 Ma to the present. Restoration of our lithospheric-scale cross section is presented for six key intervals: Present ~20 Ma, early Oligocene ~34 Ma; middle Eocene ~47 Ma; early Paleocene ~47 Ma; Maastrichtian-Paleocene ~63 Ma, and late Santonian ~83 Ma. The thickness of undeformed crust below both Aquitaine (~30 km) and Ebro foreland basins (~35 km) are those inferred from the ECORS experiment [*Choukroune and ECORS-Pyrenees Team*, 1989; *Roure et al.*, 1989]. Exploration wells used in the study are shown as vertical thick black lines on the present configuration of the Pyrenees. N: Gavarnie-Nogueres; O: Orri; R: Rialp; 3S: Trois Seigneurs; Az: Arize. Graphs on the right show temporal evolution of shortening in the Pyrenees and Iberian Ranges that is assumed to represent the total convergence between Iberia Plate relative to Europe. The preorogenic configuration crustal and lithosphere thicknesses of Iberian and European margins are constrained, assuming variable but thinning factors β lower than 2 (see Table 2). Present-day constraints on the deep structure are from LAB depth (lithosphere-asthenosphere boundary) defined by resistivity data [*Campanyà et al.*, 2011] and new *P* wave tomography (see Figure 14).

Table 2. Table Summarizing Parameters Adopted to Estimate the Mantle Lithosphere Thickness Below the Iberian and European Proximal Margins at Albo-Cenomanian, Together With Paleobathymetry/Altitude for Each Reconstructed Segment of the Pyrenees[a]

Tectonic Units	Ebro Basin	Ager and Tremp Basins	Organya Basin	Nogueres Units	Trois Seigneurs	Arize	Aquitaine Basin
Width (km)	71	38	48	32	20	27	63
Paleoelevation (km)	0	−0.1	−0.2	0	−0.5	−0.2	0
Crustal thickness H_c (km)	34.5	32	29	25	14	20	29
Upper mantle thickness H_{lm} (km)	88	83	79	88	28	40	49
Lithospheric thickness (km)	122	115	108	113	42	60	78
β factor	1	1.05	1.1	1	1.8	1.2	1

[a] $\rho_w = 1030$ kg/m^3; $\rho_{asth} = 3200$ kg/m^3; $\rho_{mant} = 3250$ kg/m^3; $\rho_{cr} = 2850$ kg/m^3. Paleobathymetry and the original crustal thickness is used to estimate the beta factors such that $\beta = H_{lm}^r/H_{lm} = H_c^r/H_c$ where H_{lm}^r and H_{lm}^r, H_{lm} and H_c are the restored and present lithospheric and crustal thickness, respectively. In this calculation, we assume pure-shear and homogeneous thinning between crust and lithospheric mantle.

emplaced at 35 Ma, an increased of incoming fluxes may have two different origins. If Model A is preferred, this could be related to the indentation of the subducting Iberian basement below the Axial Zone, thus reactivating deformation in the Orri unit [*Beaumont et al*., 2000; *Erdős et al*., 2014]. Otherwise, as suggested by *Huyghe et al*. [2009], rapid exhumation requires an external climatic forcing at the Eocene-Oligocene boundary. This interpretation may reconcile the observation of the progressive reduction of shortening in the wedge, backstepping of thrust activity and the retrogradation of continental deposits toward the Axial Zone. A third explanation, not yet explored, is the growth of dynamic topography possibly triggered by Late Eocene to Early Oligocene slab rollback in the Mediterranean [*Jolivet and Facenna*, 2000].

A late stage of deformation is apparent in the NPZ at circa 33 Ma as outlined by folding-related progressive unconformities. Shortening across the Mas d'Azil anticline is ~5 km (Figure 13). AFT data are too scarce to provide a clear picture of thrust-related exhumation above the NPFT or to confirm the possible role of climate. The youngest AFT cooling age of 37 Ma found in the Arize Massif suggests a maximum exhumation of 2–3 km (assuming 30°C/km geothermal gradient). Assuming exhumation corresponds to the movement above the existing NPFT ramp dipping 30° we roughly derive a horizontal displacement of 3.5–5 km.

We infer a total amount of shortening for this period of 20 km, with the main component accommodated in southern Pyrenees in the Rialp unit. The shortening in the northern Pyrenees is accommodated by thrusting along the NPFT. This amount contrasts with that of *Beaumont et al*. [2000] in which a total shortening of 75 km is reconstructed since the Priabonian (36 Ma) or 45 km since (30 Ma). These differences are maximum and minimum bounds that reflect whether Isona-1 well is considered in the reconstruction or not (see section 5.2 for details).

4.3.2. Middle Eocene to Early Oligocene (47–34 Ma): Crustal Stacking and Thrust Wedge Widening

Deformation in the outer SPZ is accommodated by the emplacement of the Montsec thrust and onset of deformation in the frontal units of the Sierras Marginales. Both the exhumation of the Maladeta Massif of the Orri unit and Riberot pluton in the Nogueres unit are thought to have shared the same low exhumation rates of 0.2 km/Myr from 44 to 35 Ma, as inferred from one age-elevation profile from the Riberot Massif [*Fitzgerald et al*., 1999]. Although thermal histories were probably different for both units more low-temperature constraints are needed. In the NPZ, convergence is accommodated by thrusting in the hanging wall of the NPFT and distributed shortening within NP crystalline massifs and Albo-Cenomanian basin. Our study combined with that of *Fitzgerald et al*. [1999] suggests exhumation in the northern Pyrenees from ~70 Ma until 36 Ma at a rate of ~0.2 km/Myr. Using the approach presented above, we infer a minimum cumulative shortening of 5 km above the NPFT, in the range of value proposed in other interpretation [*Beaumont et al*., 2000]. Again, shortening was essentially accommodated in the southern Pyrenees. Low-temperature and stratigraphic data indicate that starting from 50 Ma all tectonic units composing the Pyrenean orogenic wedge were active. This led to the growth of the topography up to altitude close to 2000 m at 41–49 Ma, as indicated by paleoelevation estimates [*Huyghe et al*., 2012a].

Figure 13 shows that accretion focuses on the southern Pyrenees, consistent with the asymmetric growth of the orogen. As a result of the southward migration of thrusting and/or indentation by the upper plate, subsidence rates are maximum in the southern foreland basin. On the other hand, the shortening in the northern Pyrenees is localized along the NPFT ramp, thus revealing little accretion. The different pattern of accretion may explain the limited outward migration of the flexural wave in the northern Pyrenees [*Naylor and Sinclair*, 2008]. We infer a total shortening of 20 km close to that originally proposed [*Beaumont et al*., 2000].

4.3.3. Early Paleocene to Middle Eocene (63–47 Ma): Southward Propagation and Crustal Stacking

This stage records the ongoing exhumation of the Nogueres unit associated with the onset of Montsec thrust. Transition from burial of the Maladeta Massif (Orri unit), below the Nogueres unit, to onset of cooling occurred at 50 Ma [*Metcalf et al*., 2009]. This is also documented in southern proforeland strata by a marked subsidence at 54–52 Ma. The increase of ZHe lag times between ~65 Ma and ~40 Ma further suggests decreasing exhumation rates [*Filleaudeau et al*., 2011]. However, modeling of our AFT grain age populations from the northern Pyrenees rather indicates a continuous cooling event since 70–75 Ma and ongoing shortening (Figure 10). Based on these constraints, we suggest that 20 km of shortening was accommodated in the northern Pyrenees. The remaining shortening was accommodated by both internal deformation in the Nogueres unit and thrusting along the Montsec frontal unit. Internal deformation in Nogueres unit may reflect the rheological properties of this unit, originally positioned in the most extended part of the Iberian margin. As a result, thrust movement is not entirely transferred upsection into the shallow thin-skinned deformation of the SPZ.

This period reflects a major change in the dynamics of the orogenic wedge. The accretion/exhumation of the Orri unit in the southern Pyrenees and outward propagation and accretion/exhumation of the Arize Massif accounts for wedge widening. Increasing flexural subsidence occurred in both forelands at this time; acceleration is most apparent after 50 Ma [*Sinclair et al*., 2005; *Naylor and Sinclair*, 2008]. We estimate a shortening magnitude of 32 km, which is slightly higher than the value of 25 km obtained for a shorter period ranging between 60 and 50 Ma [*Beaumont et al*., 2000].

4.3.4. Late Campanian to Early Paleocene (71–63 Ma): Onset of Tectonic Inversion

Detrital AFT data from proximal deposits of the south central Pyrenees and thermal modeling of thermochronological data from Orri unit document a cooling phase in the Nogueres unit at 70–60 Ma [*Metcalf et al*., 2009; *Beamud et al*., 2011; *Rahl et al*., 2011]. Growth strata in Late Campanian sandstones ~72 Ma [*Bond and McClay*, 1995; *Rahl et al*., 2011] are consistent with onset of Boíxols thrust and exhumation of the Nogueres basement [*Whitchurch et al*., 2011; *Filleaudeau et al*., 2011]. Our AFT data and modeling also confirm cooling by 70–75 Ma (Figure 10). Together with the pattern of ZHe data from this study and scarce ZFT ages reported from the northern Pyrenees [*Whitchurch et al*., 2011], consistent low-temperature thermochronological data between the northern and southern Pyrenees suggest that the space between the European and Iberian continent was suturing at 75–70 Ma. Mountain building started to be more apparent at that time. In the southern Pyrenees, this reflected in the deposition of 1 km thick Santonian-Campanian turbidites, topped by 400 m of latest Cretaceous/Paleocene "Garumnian" continental fluvial deposits and lacustrine limestones [e.g., *Bond and McClay*, 1995; *Ardèvol et al*., 2000; *Rosell et al*., 2001]. This is also suggested in the northern Pyrenees by the coarsening-upward succession of Campanian age in the northern foreland basin (Corbières) [*Christophoul et al*., 2003]. Based on our reconstruction, we finally estimate an amount of shortening of about 20 km during the period ranging between 70 and 63 Ma (Figure 13).

4.3.5. Santonian to Late Campanian (84–71 Ma): Collisional Suturing

Shortening since the Coniacian-Santonian cannot be directly deduced from balanced cross sections because this would necessitate restoring the suture domain. We hereafter discuss lower and upper bounds for crustal shortening that can be constrained from the temporal evolution of the Pyrenees. Westward, tectonostratigraphic relationships in the Cotiella Massif indicate that thrusting may have started in the Late Santonian ~83 Ma in the Lakhora unit [*McClay et al*., 2004]. In the northern Pyrenees, our low-temperature thermochronological data (ZHe) reveal cooling at 82 Ma. More generally this ZHe age is represented by a group of zircon grains ranging between 80 Ma and 105 Ma. The HT Pyrenean metamorphism lasted also between 110 and 85 Ma [*Albarède and Michard-Vitrac*, 1978; *Montigny et al*., 1986] and was associated with K volcanism [*Montigny et al*., 1986]. We interpret these age constraints as diagnostic of a transitional period ranging from 83 Ma to 75 Ma at the beginning of convergence. During this period cooling occurred in abnormally hot Mesozoic basins positioned on the highly extended crust of the European margin. Stretching lineations in that domain [*Choukroune*, 1974] reveal ductile shortening induced by prevailing HT conditions in the NPZ. Overall, these data are coincident with generally proposed age of the onset of convergence in the Pyrenees. Our data indicate this period is the time at which the hyperextended domain was closing. It terminates when the thicker portions of the continental margins collided at 75–70 Ma. In our reconstruction we assume that thin-skinned shortening prevailed during inversion of the hyperextended domain (Figure 13). At present, little field arguments are preserved in the suture zone to confirm this possibility. The accreted preorogenic sediments may have been eroded away or subducted. More field investigation and subsurface geophysical data will be needed to advance on this question.

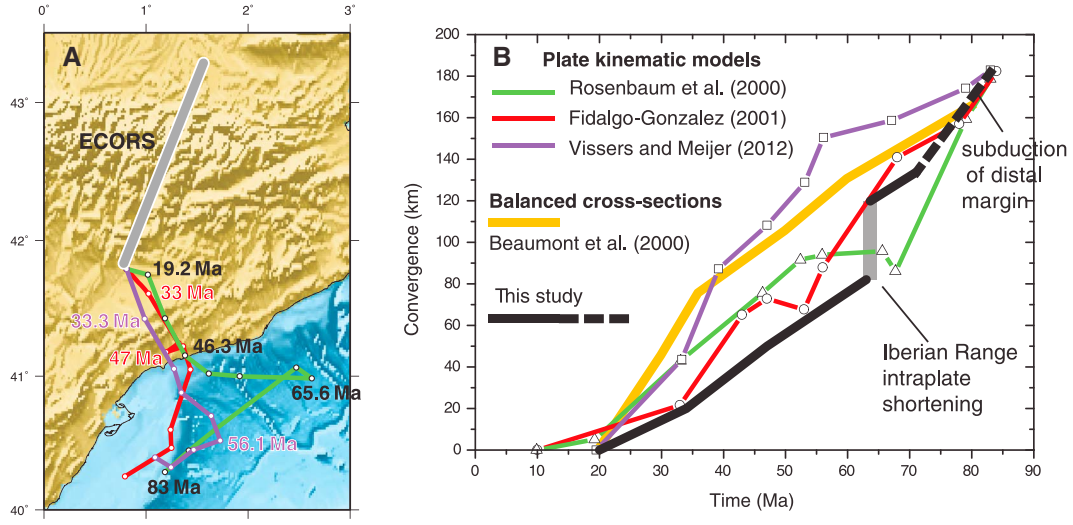

Figure 15. Comparison between convergence history inferred from three-plate kinematic models and shortening reconstructed in Figure 13. (a) Motion of Iberia relative to Europe since the start of convergence at 83 Ma. The figure show trajectories of a point (0.8075°E, 41.7925°N) currently positioned at the southern tip of the ECORS profile. Results are plotted as a function of time for three distinct kinematic reconstructions. (b) Plot showing the position of the same point on Iberia Plate relative to Europe. Distances have been projected in the direction of the ECORS profile to show the arc-normal component of convergence. These histories are compared with shortening inferred from balanced cross sections. We have distinguished between shortening inferred from balanced cross section since the beginning of cooling at 75–70 (gray line) from shortening of ~50 km that corresponds to the early stage of underthrusting needed to account for total convergence of 180 km (gray dashed line). The offset in our model corresponds to the component of shortening taken in the Iberian Range after 63 Ma.

5. Discussion

5.1. Temporal Evolution of Shortening and Implications for Kinematic Reconstructions

We infer from the reconstructions of Figure 13 a shortening of 92 km across the central Pyrenees. This amount is in the low range of published shortening estimates [*Roure et al*., 1989; *Teixell*, 1998; *Vergés et al*., 2002; *Martinez-Peña and Casas-Sainz*, 2003] and is noticeably lower than shortening of 165 km [*Beaumont et al*., 2000]. In the following, we compare the temporal distribution of shortening implied by our sequential restoration (Figure 15) and that of *Beaumont et al*. [2000] with plate kinematic constraints [*Olivet*, 1996; *Fidalgo González*, 2001; *Rosenbaum et al*., 2002; *Vissers and Meijer*, 2012a, 2012b] as defined by plate tectonic rotation parameters of Table 3.

First, we must consider intraplate shortening in the Iberian Plate that is not reproduced in our restoration. *Guimera et al*. [2004] estimated a shortening between 38 and 66 km since Late Cretaceous, in the Iberian Range. The range of shortening estimates reflects different interpretations of the deep geometry of basement thrust ramp. A lower value of 40 km is preferred, here, which has the quality of being in better agreement with midcrustal detachment and thick-skin deformation characteristics of the Iberian Range [*de Vicente et al*., 2007]. Among the total IB/EU convergence of ~180 km, these 40 km of shortening were accommodated from the Paleogene (~63 Ma) to the early Miocene (~20 Ma). This deformation must be added to the cumulated shortening of ~70 km after 63 Ma as proposed in our study. This provides an explanation for the differences between Beaumont's reconstruction and ours after 63 Ma. Prior to 63 Ma, ~70 km of shortening has to be accommodated in the Pyrenees. This amount was variably accommodated by crustal accretion and north directed subduction of the distal extremely thinned margin. Among them, 20 km was taken up between 71 and 63 Ma with a transition toward accretion of more proximal segments of the margins as suggested by cooling after 70–75 Ma and tectonostratigraphic data in the forelands. The remaining ~50 km of shortening were therefore accommodated by subduction.

Figure 15 shows that restorations from *Beaumont et al*. [2000] and ours conform both with a total convergence of ~180 km since the Santonian. However, the deformation histories are quite different. *Beaumont et al*. [2000] assume highest shortening rates (~4.5 km/Myr) after 40 Ma, but we place the most rapid shortening rates at the onset of convergence at 80–60 Ma (~3.5 km/Myr) reducing to about 2 km/Myr as

Table 3. Euler Poles of Rotation and Finite Rotation Angles and Best Fitting Kinematic Parameters for Models R2002 of *Rosenbaum et al.* [2002], F2001 of *Fidalgo González* [2001], and V&M of *Vissers and Meijer* [2012a]

	Age (Ma)	Latitude (°N)	Longitude (°W)	Rotation (deg)
Model R2002	9.9	0	0	0
	19.2	77.93	59.14	0.24
	33.1	−31.21	166.79	1.73
	46.3	−23.85	157.12	1.72
	52.4	−21.6	157.88	2.1
	55.9	−20.72	162.4	2.61
	65.6	−12.95	165.77	3.02
	67.7	−16.45	167.49	3.1
	79.1	−37.17	169	8.04
	83	−38.86	169.85	10
Model F2001	10	0	0	0
	33	33.14	−9.91	−1.16
	43	33.55	−11.43	−3.05
	47	36.13	−11.2	−3.6
	53	34.21	−10.08	−3.57
	56	34.95	−10.2	−4.61
	68	36.83	−14.23	−5.65
	78	38.15	−10.94	−8.12
	84	40.43	−11.49	−9.49
Model V&M	19.5	0	0	0
	33.3	−31.77	161.02	1.302
	39.2	−14.1	140.1	1.16
	47	−30.59	158.88	2.81
	53.1	−29.15	160.91	3.591
	56.1	−28.68	159.71	3.941
	67.1	−35.27	165.43	6.061
	79	−37.67	166.88	7.597
	83	−39.36	170.34	9.8

shortening is transferred to the Iberian Range at 63 Ma. Both reconstructions are overall consistent on the interval 60–40 Ma, showing stable shortening rates of ~2 km/Myr.

The deformation rates history inferred from our reconstruction (Figure 15b) better fits with models proposed by *Rosenbaum et al*. [2002] or *Fidalgo González* [2001]. These models assume an initially rapid convergence at 83 Ma with a marked slowdown at 65–50 Ma. Such a reduction in the rates of convergence in the North-South direction expresses significant strike-slip motion (Figure 15a). This is seen to occur slightly later for *Fidalgo González* [2001] at 53–43 Ma. The generally decreasing rates of shortening and the sharp change at 63 Ma related to the migration of deformation in the Iberian Range agree with the two reconstructions cited above. This result is in marked contrast with *Vissers and Meijer* [2012a] in which the initial convergence is rather slow, then accelerated at 60 Ma then at 40 Ma.

We infer that a cross section of the central Pyrenees implying minimum shortening of ~90 km may be reconciled with plate reconstructions if strain is partitioned between intraplate deformation (40 km), subduction of the extremely thinned margin (from 50 km), and crustal thickening in the Pyrenees (90 km) (Figure 16). Our scenario accounts for most recent geological models from the northern Pyrenees in which a domain of hyperextension, formed during divergence between Iberia and Europe, has been recognized [*Jammes et al*., 2009; *Lagabrielle et al*., 2010]. It reproduces well time-temperature constraints indicating a most significant cooling starting after 75–70 Ma. Although the constraints presented in this study are

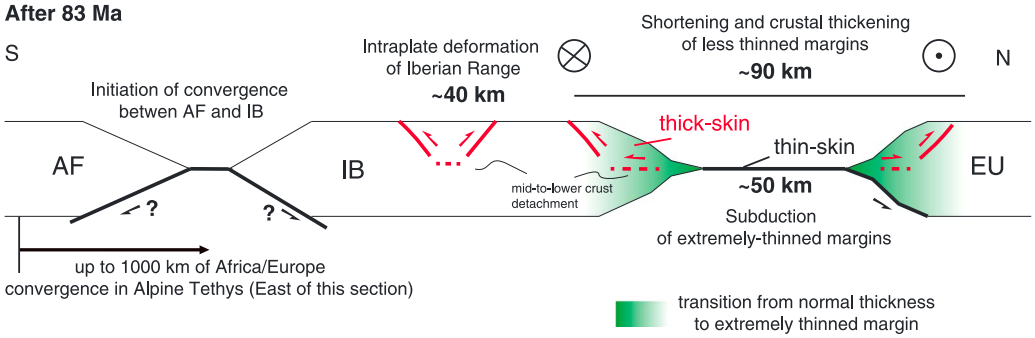

Figure 16. Strain distribution in the Africa/Iberia/Europe plate framework as inferred from the Pyrenean shortening (in roughly North-South direction, parallel to the ECORS profile). IB/EU plate convergence of 180 km is accommodated between intraplate deformation in the Iberian Range, underthrusting of distal margin (thin-skin deformation) and crustal thickening (thick-skin deformation in red). Africa moved faster northward in the Alpine region by accommodating up to 1000 km of convergence since 83 Ma [*Capitanio and Goes*, 2006].

representative of the evolution of the central Pyrenees only, the amount of shortening is consistent with other estimates in the Pyrenees [*Roure et al*., 1989; *Vergés et al*., 1995; *Teixell*, 1998; *Martinez-Peña and Casas-Sainz*, 2003]. The timing and amount of underthrusting of the distal margin may however vary along the strike of the belt due to variable amount of extension and rift-related margin architecture.

Overall, a limited intraplate and Pyrenean shortening agree with kinematic models in which the main part of the Africa/Iberia convergence relative to Europe since 84 Ma of at least 1000 km was accommodated further to the East in the Alpine Tethys [*Capitanio and Goes*, 2006; *Handy et al*., 2010]. During our studied time interval, Africa was moving relative to Iberia but the exact nature of the deformation at the plate boundary is debated. Ages of peak HP metamorphism in the Betics imply Late Cretaceous continental subduction south of Iberia. In the Late Cretaceous, models include either a South dipping subduction of the Tethys below North Africa [*Vergés and Fernàndez*, 2012] or a North dipping subduction [*Sainz and Faccenna*, 2001]. Other models suggest a transitional plate boundary between strike slip and extensional since the Late Jurassic [*Schettino and Turco*, 2010] or purely strike slip along a transform fault boundary [*Rosenbaum et al*., 2002; *Sibuet et al*., 2004; *van Hinsbergen et al*., 2014]. These models pose the question of the driving forces at the origin of the North-South collisional shortening in the Pyrenees and intra-Iberia shortening.

5.2. Transition From Subduction To Collision in the Pyrenees: The Role of Margin Architecture

Crustal accretion that contributes to the growth of the orogenic wedge reflects ~30% of shortening (ratio of shortening to the length of the restored section). This value is in general agreement with shortening expected for thrust belts built on lithosphere with Peri-Tethyan Mesozoic thermotectonic ages [*Mouthereau et al*., 2013]. It illustrates a dominant thick-skin deformation style characterized by vertically distributed strain within the Iberian and European crust above middle-to-lower crustal ramps and décollement. Such weak crustal layers are thought to be absent in more thinned distal margin due to shear localization in the middle crust [*Mohn et al*., 2012] or lower crustal flow [*Brune et al*., 2014] in the necking domain. The distal margin is also denser. This probably explains prominent underthrusting of this part of the margin of which we have increasing evidence, for instance, from geophysical data in active Taiwan orogen [*McIntosh et al*., 2013; *Eakin et al*., 2014] or suggested from tectonic reconstructions in the Zagros [*Mouthereau et al*., 2012].

We interpreted our ZHe data and AFT models suggest a relatively slow cooling period from 105 to 75 Ma, followed by faster cooling after 75–70 Ma (5.5°C/Myr). The first period is transitional between the timing of maximum crustal thinning in the Albian, and the onset of plate convergence at 83 Ma. This may reflect a period of underthrusting/shortening of originally hot and thin portions at the suture zone and near the NPFT. In the NPZ, it has been suggested that a significant part if not all the ductile deformation observed in Mesozoic basins could have occurred during this critical period [*Vacherat et al*., 2014]. This study carried out in Albo-Cenomanian Mauléon Basin of Western Pyrenees reveals that rift-related high geothermal gradients (~80°C/km) inherited from crustal breakup at 100 Ma were maintained over a period of 20–30 Myr after onset of convergence.

The inversion of Mesozoic basins during the late Santonian is recorded in the southern Pyrenees (e.g., Cotiella Massif). This occurred coevally with the movement of the Riberot or Eaux-Chaudes/Lakhora (Figure 13). However, significant foreland subsidence did not seem to have occurred before 70 Ma, consistent with our AFT ages indicating the onset of cooling rates after 75–70 Ma. The transition from underthrusting to accretion of the less thinned portions of the continental margins may be responsible for the acceleration of cooling observed.

In our restoration (Figures 13 and 15) we have proposed that during the earliest stage of convergence, the deformation was accommodated by thin-skin shortening (shallow crust)/subduction (lithospheric mantle) of the distal Iberian margin to the south and by thrusting above the NPFT in the north. As the proximal margins of Iberia and Europe came into contact, thick-skin shortening started to involve deep crustal décollement and inherited north dipping Hercynian thrust ramps. This marks the onset of the growth of the doubly vergent orogenic wedge.

As illustrated in Figure 13, the transition from continental underthrusting to collisional thickening in the latest Cretaceous reflects the juxtaposition of Iberia and Europe lithospheres of different thicknesses and properties along the North Pyrenean Fault (i.e., the suture region). This variation likely illustrates evolution of the NPF as a transform margin that underwent hyperextension during the Albian. This is supported in several

aspects by the most recent geological studies [*Lagabrielle and Bodinier*, 2008; *Jammes et al*., 2009; *Lagabrielle et al*., 2010; *Clerc et al*., 2012; *Vauchez et al*., 2013]. We infer that initiation of the continental subduction started at 83 Ma at a transform plate boundary. Our model agrees with a relatively limited subduction prior to 83 Ma in accordance plate reconstruction proposed by *Jammes et al*. [2009] or *Olivet* [1996]. Rifting in the Albian caused by extensional boundary conditions agrees with cooling history, indicating cooling from 105 Ma. The lack of geological and geophysical evidence throughout the Pyrenees for 300 km subduction of Neotethyan ocean, slab foundering and detachment in the Pyrenees at 120–83 Ma [*Souriau et al*., 2008; *Chevrot et al*., 2014a] lead us not to favor the model of *Vissers and Meijer* [2012a].

Upper bounds for shortening since 83 Ma may be otherwise preferred [*Beaumont et al*., 2001], but it does not leave room for the extreme thinning induced by North-South extension in Middle Cretaceous documented in the Pyrenees. Alternatively, crustal thinning and mantle exhumation may have occurred in narrow/deep rhomboidal Albian-Cenomanian flysch basins along the NPF [*Clerc et al*., 2012], which would reduce the amount of North directed subduction. Overall, our model and the increasing number of new geological and geophysical constraints in the Pyrenees support North-South extension, including the development of 70–50 km of extremely thinned domain in the Albian, along the NPF, an older transform plate boundary. The lack of significant convergence prior to 83 Ma, in the Pyrenees reveals the need for the revision of pre-83 Ma Iberia plate motion as discussed recently [*Bronner et al*., 2011].

We show that initiation of underthrusting few Myr after extreme thinning explains apparent underevaluation of shortening after 83 Ma using balanced cross sections. This study demonstrates the key role tectonic inheritance, and in particular rift-related margin architecture, play in plate reconstructions.

6. Conclusion

In this paper, we aimed to evaluate the role of the margin architecture in the shortening history of the Pyrenees, discuss higher and lower bounds of crustal shortening inferred from balanced cross sections, and examine implications for plate kinematic reconstructions. We have reconstructed shortening evolution in the Pyrenees by taking into account past and recent geological data, as well as new low-temperature detrital thermochronology constraints from the northern Pyrenees.

We show that following extension in the Albian (~110 Ma), an extremely thinned domain of the northern Iberia margin underwent a limited North directed subduction (50 km) starting at 83 Ma. The proposed reconstruction fits well with an initiation of convergence at a transform plate boundary, the North Pyrenean Fault. This model implies the opening of a minimum 50 km wide basin at the distal margins of Iberia/Europe plates during the Albian, which provides support for a North-South extension along the NPF. Both constraints are best reconciled by temporally decouple, strike-slip movement and North-South extension along the North Pyrenean Fault. This implies that the eastward displacement of Iberia must have occurred before the Albian hyperextension. There is evidence of prebreakup extension of about 400 km between Newfoundland and Galicia margins during the Jurassic and before oceanic accretion in the Albian [e.g., *Sutra et al*., 2013; *Reston and McDermott*, 2014] in agreement with *Jammes et al*. [2009].

The earliest stage of convergence at the distal margin occurred from 83 Ma to 71 Ma. Evidence for this early stage is lacking but corresponding deformation must be found close to the suture zone and HT metamorphic domain in the vicinity of the North Pyrenean Fault. Due to the originally hot extensional basins in the northern Pyrenees, shortening occurred in the ductile regime. High geothermal gradient on the distal margin is supported by the range of AFT and ZHe thermochronological ages that overall suggest slow cooling prior to 75–70 Ma. We proposed that such cooling, which is consistent with previous constraints from the south, marks the transition from convergence of the highly extended distal margin (collisional suturing) that leaves little information at the surface, to the main episode of orogenic growth. From 71 to 20 Ma about 90 km of crustal shortening contribute to the building of the collision belt and account for long-lived south migrating exhumation of Iberian and European basement units and development of foreland basins.

We conclude that relatively low crustal shortening of 90 km (30%) reflects the dominant thick-skin tectonic style of shortening during collision of European and Iberian margins. This is in agreement with shortening expected for proximal margins that have preserved a ductile middle-to-lower crust able of be activated as deep decoupling level during convergence. This study suggests that plate reconstructions that use

nonunique scenario of shortening evolution from balanced cross section should evaluate their hypotheses in the light of shortening predicted by inherited age-dependent properties of the continental lithosphere.

Acknowledgments
This study was supported by French National Research Agency (PYRAMID)—ANR-11-BS56-0031. Data supporting Figures 8 and 11 are available as Tables S1 and S2 in the supporting information. We thank S. Chevrot for providing the *P* wave tomography data of Figure 14 and sharing other recent results from the PYROPE project.

References

Albarède, F., and A. Michard-Vitrac (1978), Age and significance of the North Pyrenean metamorphism, *Earth Planet. Sci. Lett.*, *40*(3), 327–332.
Ardèvol, L., J. Klimowitz, J. Malagon, and P. J. C. Nagtegaal (2000), Depositional sequence response to foreland deformation in the Upper Cretaceous of the southern Pyrenees, Spain, *Bulletin*, *84*(4), 566–587.
Babault, J., J. Van den Driessche, S. Bonnet, S. Castelltort, and A. Crave (2005), Origin of the highly elevated Pyrenean peneplain, *Tectonics*, *24*, TC2010, doi:10.1029/2004TC001697.
Babault, J., N. Loget, J. van den Driessche, S. Castelltort, S. Bonnet, and P. Davy (2006), Did the Ebro Basin connect to the Mediterranean before the Messinian salinity crisis?, *Geomorphology*, *81*, 155–165.
Baby, P. (1988), Chevauchements dans une zone à structure complexe: La zone nord-pyrénéenne ariégeoise, PhD, Université Paul Sabatier Toulouse III, 145 p.
Beamud, E., J. A. Muñoz, P. G. Fitzgerald, S. L. Baldwin, M. Garcés, L. Cabrera, and J. R. Metcalf (2011), Magnetostratigraphy and detrital apatite fission track thermochronology in syntectonic conglomerates: Constraints on the exhumation of the south-central Pyrenees, *Basin Res.*, doi:10.1111/j.1365-2117.2010.00492.x.
Beaumont, C., J. A. Muñoz, J. Hamilton, and P. Fullsack (2000), Factors controlling the Alpine evolution of the central Pyrenees inferred from a comparison of observations and geodynamical models, *J. Geophys. Res.*, *105*(B4), 8121–8145, doi:10.1029/1999JB900390.
Bellahsen, N., F. Mouthereau, A. Boutoux, M. Bellanger, O. Lacombe, L. Jolivet, and Y. Rolland (2014), Collision kinematics in the western external Alps, *Tectonics*, *33*, 1055–1088, doi:10.1002/2013TC003453.
Beràstegui, X., J. M. García-Senz, and M. Losantos (1990), Tecto-sedimentary evolution of the Organya extensional basin (central south Pyrenean unit, Spain) during the Lower Cretaceous, *Bull. Soc. Geol. Fr.*, *VI*(2), 251–264, doi:10.2113/gssgfbull.VI.2.251.
Biteau, J.-J., A. Le Marrec, M. Le Vot, and J.-M. Masset (2006), The Aquitaine Basin, *Petrol. Geosci.*, *12*, 247–273.
Bodinier, J. L., and M. Godard (2007), 2.04—Orogenic, ophiolitic, and abyssal peridotites, in *Treatise on Geochemistry*, edited by D. H. Heinrich and K. T. Karl, pp. 1–73, Pergamon, Oxford, U. K.
Bond, R. M. G., and K. R. McClay (1995), Inversion of a Lower Cretaceous extensional basin, south central Pyrenees, Spain, *Geol. Soc. London Spec. Publ.*, *88*(1), 415–431, doi:10.1144/GSL.SP.1995.088.01.22.
Boulvais, P., G. Ruffet, J. Cornichet, and M. Mermet (2007), Cretaceous albitization and dequartzification of Hercynian peraluminous granite in the Salvezines Massif (French Pyrénées), *Lithos*, *93*(1–2), 89–106, doi:10.1016/j.lithos.2006.05.001.
Bronner, A., D. Sauter, G. Manatschal, G. Peron-Pinvidic, and M. Munschy (2011), Magmatic breakup as an explanation for magnetic anomalies at magma-poor rifted margins, *Nat. Geosci.*, *4*(8), 549–553, doi:10.1038/nphys1201.
Brune, S., C. Heine, and M. Pérez-Gussinyé (2014), Rift migration explains continental margin asymmetry and crustal hyper-extension, *Nature*, doi:10.1038/ncomms5014.
Byrne, T., Y. C. Chan, R. J. Rau, C. Y. Lu, Y. H. Lee, and Y. J. Wang (2011), The Arc-Continent collision in Taiwan, in *Frontiers in Earth Sciences*, pp. 213–245, Springer, Berlin.
Campanyà, J., J. Ledo, P. Queralt, A. Marcuello, M. Liesa, and J. A. Muñoz (2011), Lithospheric characterization of the central Pyrenees based on new magnetotelluric data, *Terra Nova*, *23*(3), 213–219, doi:10.1111/j.1365-3121.2011.01001.x.
Capitanio, F. A., and S. Goes (2006), Mesozoic spreading kinematics: Consequences for Cenozoic central and western Mediterranean subduction, *Geophys. J. Int.*, *165*(3), 804–816, doi:10.1111/j.1365-246X.2006.02892.x.
Castiñeiras, P., M. Navidad, M. Liesa, J. Carreras, and J. K. Casas (2008), U-Pb zircon ages (SHRIMP) for Cadomian and Early Cadomian magmatism in the Eastern Pyrenees: New insights into the pre-Variscan evolution of the northern Gondwana margin, *Tectonophysics*, *461*, 228–239.
Chevrot, S., et al. (2014a), High resolution imaging of the Pyrenees and Massif central from the data of the PYROPE and IBERARRAY portable array deployments, *J. Geophys. Res. Solid Earth*, *119*, 6399–6420, doi:10.1002/2014JB010953.
Chevrot, S., Sylvander, M., Diaz, J., Ruiz, D., Paul, A., and the PYROPE Working Group (2014b), The Pyrenean architecture as revealed by teleseismic P-to-S converted waves recorded along two dense transects, in revision to *Geophys. J. Int.*
Choukroune, P. (1974), Structure et évolution tectonique de la Zone Nord-Pyrénéene. Analyse de la déformation dans la portion de chaîne à schistosité sub-verticale, PhD thesis, p. 246, Université des Sciences et Techniques du Langedoc, Montpellier.
Choukroune, P. (1992), Tectonic evolution of the Pyrenees, *Annu. Rev. Earth Planet. Sci.*, *20*, 143.
Choukroune, P., and the ECORS-Pyrenees Team (1989), The ECORS-Pyrenean deep seismic profile reflection data and the overall structure of the orogenic belt, *Tectonics*, *8*, 23–29, doi:10.1029/TC008i001p00023.
Choukroune, P., and M. Mattauer (1978), Tectonique des plaques et Pyrénées: Sur le fonctionnement de la faille transformante nord-pyrénéenne—Comparaison avec des modèles actuels, *Bull. Soc. Geol. Fr.*, *20*(5), 689–700.
Choukroune, P., and M. Seguret (1973), Carte structurale des Pyrénées, 1:500.000, Editions ELF-ERAP, Boussens, France.
Choukroune, P., X. Le Pichon, M. Seguret, and J.-C. Sibuet (1973), Bay of Biscay and Pyrenees, *Earth Planet. Sci. Lett.*, *18*(1), 109–118, doi:10.1016/0012-821X(73)90041-1.
Choukroune, P., B. Pinet, F. Roure, and M. Cazes (1990), Major Hercynian thrusts along the ECORS Pyrenees and Biscay lines, *Bull. Soc. Geol. Fr.*, *VI*(2), 313–320, doi:10.2113/gssgfbull.VI.2.313.
Christophoul, F., J. C. Soula, S. Brusset, B. Elibana, M. Roddaz, G. Bessiere, and J. Déramond (2003), Time, place and mode of propagation of foreland basin systems as recorded by the sedimentary fill: Examples of the Late Cretaceous and Eocene retro-foreland basins of the north-eastern Pyrenees, *Geol. Soc. London Spec. Publ.*, *208*, 229–252, doi:10.1144/GSL.SP.2003.208.01.11.
Clerc, C., and Y. Lagabrielle (2014), Thermal control on the modes of crustal thinning leading to mantle exhumation. Insights from the Cretaceous Pyrenean hot paleomargins, *Tectonics*, *33*, 1340–1359, doi:10.1002/2013TC003471.
Clerc, C., Y. Lagabrielle, M. Neumaier, J.-Y. Reynaud, and M. de Saint Blanquat (2012), Exhumation of subcontinental mantle rocks: Evidence from ultramafic-bearing clastic deposits nearby the Lherz peridotite body, French Pyrenees, *Bull. Soc. Geol. Fr.*, *183*(5), 443–459, doi:10.2113/gssgfbull.183.5.443.
Coney, P. J., J. A. Muñoz, K. R. McClay, and C. A. Evenchick (1996), Syntectonic burial and post-tectonic exhumation of the southern Pyrenees foreland fold-thrust belt, *J. Geol. Soc.*, *153*(1), 9–16, doi:10.1144/gsjgs.153.1.0009.
Copley, A., J.-P. Avouac, and J.-Y. Royer (2010), India-Asia collision and the Cenozoic slowdown of the Indian Plate: Implications for the forces driving plate motions, *J. Geophys. Res.*, *115*, B03410, doi:10.1029/2009JB006634.

Costa, E., M. Garcés, M. Lopez-Blanco, E. Beamud, M. Gomez-Paccard, and J. C. Larrasoaña (2010), Closing and continentalization of the South Pyrenean foreland basin (NE Spain): Magnetochronological constraints, *Basin Res.*, *22*(6), 904–917.

Costa, S., and H. Maluski (1988), Use of the 40Ar-39Ar stepwise heating method for dating mylonite zones: An example from the St. Barthélémy Massif (northern Pyrenees, France), *Chem. Geol. Isot. Geosci.*, *72*(2), 127–144, doi:10.1016/0168-9622(88)90061-9.

de Saint-Blanquat, M., J. M. Lardeaux, and M. Brunel (1990), Petrological arguments for high-temperature extensional deformation in the Pyrenean Variscan crust (Saint Barthélémy Massif, Ariège, France), *Tectonophysics*, *177*(1–3), 245–262, doi:10.1016/0040-1951(90)90284-f.

de Vicente, G., et al. (2007), Cenozoic thick-skinned deformation and topography evolution of the Spanish Central System, *Global Planet. Change*, *58*(1–4), 335–381, doi:10.1016/j.gloplacha.2006.11.042.

DeCelles, P. G., and P. C. DeCelles (2001), Rates of shortening, propagation, underthrusting, and flexural wave migration in continental orogenic systems, *Geology*, *29*(2), 135–138.

Deloule, E., P. Alexandrov, A. Cheilletz, B. Laumonier, and P. Barbey (2002), In-situ U-Pb zircon ages for Early Ordovician magmatism in the eastern Pyrenees, France: The Canigou orthogneisses, *Int. J. Earth. Sci. (Geol. Rundsch.)*, *91*(3), 398–405.

Denèle, Y., P. Barbey, E. Deloule, E. Pelleter, P. Olivier, and G. Gleizes (2009), Middle Ordovician U-Pb age of the Aston and Hospitalet orthogneissic laccoliths: Their role in the Variscan evolution of the Pyrenees, *Bull. Soc. Geol. Fr.*, *180*(3), 209–216.

Déramond, J., P. Souquet, M.-J. Fondecave-Wallez, and M. Specht (1993), Relationships between thrust tectonics and sequence stratigraphy surfaces in foredeeps: Model and examples from the Pyrenees (Cretaceous-Eocene, France, Spain), *Geol. Soc. London Spec. Publ.*, *71*(1), 193–219, doi:10.1144/GSL.SP.1993.071.01.09.

Desegaulx, P., F. Roure, and A. Villien (1990), Structural evolution of the Pyrenees: Tectonic inheritance and flexural behaviour in the continental crust, *Tectonophysics*, *182*(3–4), 211–225, doi:10.1016/0040-1951(90)90164-4.

Desegaulx, P., H. Kooi, and S. Cloetingh (1991), Consequence of foreland basin development on thinned continental lithosphere: Application to the Aquitaine Basin (SW France), *Earth Planet. Sci. Lett.*, *106*, 106–132.

Dewey, J. F., M. L. Helman, S. D. Knott, E. Turco, and D. H. W. Hutton (1989), Kinematics of the western Mediterranean, *Geol. Soc. London Spec. Publ.*, *45*, 265–283, doi:10.1144/GSL.SP.1989.045.01.15.

Dinarès-Turell, J., and J. García-Senz (2000), Remagnetization of Lower Cretaceous limestones from the southern Pyrenees and relation to the Iberian Plate geodynamic evolution, *J. Geophys. Res.*, *105*(B8), 19,405–19,418, doi:10.1029/2000JB900136.

Eakin, D. H., K. D. McIntosh, H. J. A. Van Avendonk, L. Lavier, R. Lester, C.-S. Liu, and C.-S. Lee (2014), Crustal-scale seismic profiles across the Manila subduction zone: The transition from intraoceanic subduction to incipient collision, *J. Geophys. Res. Solid Earth*, *119*, 1–17, doi:10.1002/2013JB010395.

Erdős, Z., P. van der Beek, and R. S. Huismans (2014), Evaluating balanced section restoration with thermochronology data: A case study from the central Pyrenees, *Tectonics*, *33*, 617–634, doi:10.1002/2013TC003481.

Farrell, S. G., G. D. Williams, and C. D. Atkinson (1987), Constraints on the age of movement of the Montsech and Cotiella thrusts, south central Pyrenees, Spain, *J. Geol. Soc.*, *144*(6), 907–914, doi:10.1144/gsjgs.144.6.0907.

Fidalgo González, L. (2001), *La cinématique de l'Atlantique Nord: La question de la déformation intraplaque*, 340 pp., Université de Bretagne Occidentale, Brest, France.

Filleaudeau, P. Y. (2011), Croissance et dénudation des Pyrénées du Crétacé Supérieur au Paléogène, PhD thesis, 334 pp., Université Pierre et Marie Curie, Paris.

Filleaudeau, P.-Y., F. Mouthereau, and R. Pik (2011), Thermo-tectonic evolution of the south-central Pyrenees from rifting to orogeny: Insights from detrital zircon U/Pb and (U-Th)/He thermochronometry, *Basin Res.*, *24*(4), 401–417, doi:10.1111/j.1365-2117.2011.00535.x.

Fillon, C., and P. van der Beek (2012), Post-orogenic evolution of the southern Pyrenees: Constraints from inverse thermo-kinematic modelling of low-temperature thermochronology data, *Basin Res.*, *24*(4), 418–436, doi:10.1111/j.1365-2117.2011.00533.x.

Fillon, C., C. Gautheron, and P. van der Beek (2013), Oligocene–Miocene burial and exhumation of the southern Pyrenean foreland quantified by low-temperature thermochronology, *J. Geol. Soc.*, *170*(1), 67–77, doi:10.1144/jgs2012-051.

Fitzgerald, P. G., J. A. Muñoz, P. J. Coney, and S. L. Baldwin (1999), Asymmetric exhumation across the Pyrenean orogen: Implications for the tectonic evolution of a collisional orogen, *Earth Planet. Sci. Lett.*, *173*, 157–170.

Galbraith, R. F., and P. F. Green (1990), Estimating the component ages in a finite mixture, *Nucl. Tracks Radiat. Meas.*, *17*, 197–206.

Galbraith, R. F., and G. M. Laslett (1993), Statistical models for mixed fission track ages, *Int. J. Radiat. Appl. Instrum. Nucl.Tracks Radiat. Meas.*, *21*(4), 459–470.

Gallagher, K. (2012), Transdimensional inverse thermal history modeling for quantitative thermochronology, *J. Geophys. Res.*, *117*, B02408, doi:10.1029/2011JB008825.

Gallagher, K., K. Charvin, S. Nielsen, M. Sambridge, and J. Stephenson (2009), Markov chain Monte Carlo (MCMC) sampling methods to determine optimal models, model resolution and model choice for Earth Science problems, *Mar. Petrol. Geol.*, *26*(4), 525–535, doi:10.1016/j.marpetgeo.2009.01.003.

Garcia-Castellanos, D., J. Vergés, J. Gaspar-Escribano, and S. Cloetingh (2003), Interplay between tectonics, climate, and fluvial transport during the Cenozoic evolution of the Ebro Basin (NE Iberia), *J. Geophys. Res.*, *108*(B7), 2347, doi:10.1029/2002JB002073.

García-Sansegundo, J., J. Poblet, J. L. Alonso, and P. Clariana (2011), Hinterland-foreland zonation of the Variscan orogen in the Central Pyrenees: Comparison with the northern part of the Iberian Variscan Massif, *Geol. Soc. London Spec. Publ.*, *349*(1), 169–184, doi:10.1144/sp349.9.

García-Senz, J. (2002), *Cuencas Extensivas del Cretacico Inferior en los Pirineos Centrales, Formación y Subsecuente Inversión*, 310 pp., Univ. of Barcelona, Spain.

Gibson, M., H. D. Sinclair, G. J. Lynn, and F. M. Stuart (2007), Late- to post-orogenic exhumation of the central Pyrenees revealed through combined thermochronological data and modelling, *Basin Res.*, *19*, 323–334, doi:10.1111/j.1365-2117.2007.00333.x.

Golberg, J. M., and A. F. Leyreloup (1990), High temperature-low pressure Cretaceous metamorphism related to crustal thinning (eastern north Pyrenean zone, France), *Contrib. Mineral. Petrol.*, *104*(2), 194–207, doi:10.1007/BF00306443.

Gong, Z., C. G. Langereis, and T. A. T. Mullender (2008), The rotation of Iberia during the Aptian and the opening of the Bay of Biscay, *Earth Planet. Sci. Lett.*, *273*, 80–93, doi:10.1016/j.epsl.2008.06.016.

Guimera, J., R. Mas, and Á. Alonso (2004), Intraplate deformation in the NW Iberian Chain: Mesozoic extension and Tertiary contractional inversion, *J. Geol. Soc.*, *161*(2), 291–303.

Handy, M. R., S. M. Schmid, R. Bousquet, E. Kissling, and D. Bernoulli (2010), Reconciling plate-tectonic reconstructions of Alpine Tethys with the geological–geophysical record of spreading and subduction in the Alps, *Earth Sci. Rev.*, *102*(3–4), 121–158, doi:10.1016/j.earscirev.2010.06.002.

Hurford, A. J., and P. F. Green (1983), The zeta age calibration of fission-track dating, *Chem. Geol.*, *41*, 285–317.

Huyghe, D., F. Mouthereau, S. Castelltort, P. Y. Filleaudeau, and L. Emmanuel (2009), Paleogene propagation of the southern Pyrenean thrust wedge revealed by finite strain analysis in frontal thrust sheets: Implications for mountain building, *Earth Planet. Sci. Lett.*, *288*(3–4), 421–433, doi:10.1016/j.epsl.2009.10.002.

Huyghe, D., F. Mouthereau, and L. Emmanuel (2012a), Oxygen isotopes of marine mollusc shells record Eocene elevation change in the Pyrenees, *Earth Planet. Sci. Lett.*, *345-348*(C), 131–141, doi:10.1016/j.epsl.2012.06.035.

Huyghe, D., S. Castelltort, F. Mouthereau, J. Serra-Kiel, P.-Y. Filleaudeau, L. Emmanuel, B. Berthier, and M. Renard (2012b), Large scale facies change in the middle Eocene South-Pyrenean foreland basin: The role of tectonics and prelude to Cenozoic ice-ages, *Sedimentary Geol.*, *253–254*, 25–46, doi:10.1016/j.sedgeo.2012.01.004.

Jammes, S., and R. S. Huismans (2012), Structural styles of mountain building: Controls of lithospheric rheologic stratification and extensional inheritance, *J. Geophys. Res.*, *117*, B10403, doi:10.1029/2012JB009376.

Jammes, S., G. Manatschal, L. Lavier, and E. Masini (2009), Tectonosedimentary evolution related to extreme crustal thinning ahead of a propagating ocean: Example of the western Pyrenees, *Tectonics*, *28*, TC4012, doi:10.1029/2008TC002406.

Jolivet, L., and C. Facenna (2000), Mediterranean extension and the Africa-Eurasia collision, *Tectonics*, *19*(6), 1095–1106, doi:10.1029/2000TC900018.

Jolivet, M., P. Labaume, P. Monié, M. Brunel, N. Arnaud, and M. Campani (2007), Thermochronology constraints for the propagation sequence of the south Pyrenean basement thrust system (France-Spain), *Tectonics*, *26*, TC5007, doi:10.1029/2006TC002080.

Ketcham, R. A., A. Carter, R. A. Donelick, J. Barbarand, and A. J. Hurford (2007), Improved modeling of fission-track annealing in apatite, *Am. Miner.*, *92*(5–6), 799–810, doi:10.2138/am.2007.2281.

Ketcham, R. A., C. Gautheron, and L. Tassan-Got (2011), Accounting for long alpha-particle stopping distances in (U–Th–Sm)/He geochronology: Refinement of the baseline case, *Geochim. Cosmochim. Acta*, *75*(24), 7779–7791, doi:10.1016/j.gca.2011.10.011.

Lachenbruch, A. H., and P. Morgan (1990), Continental extension, magmatism and elevation; formal relations and rules of thumb, *Tectonophysics*, *174*(1–2), 39–62, doi:10.1016/0040-1951(90)90383-J.

Lagabrielle, Y., and J. L. Bodinier (2008), Submarine reworking of exhumed subcontinental mantle rocks: Field evidence from the Lherz peridotites, French Pyrenees, *Terra Nova*, *20*(1), 11–21, doi:10.1111/j.1365-3121.2007.00781.x.

Lagabrielle, Y., P. Labaume, and M. de Saint-Blanquat (2010), Mantle exhumation, crustal denudation and gravity tectonics during Cretaceous rifting in the Pyrenean realm (SW Europe): Insights from the geological setting of the lherzolite bodies, *Tectonics*, *29*, TC4012, doi:10.1029/2009TC002588.

Lanaja, J. M. (1987), *Contribución de la Exploración Petrolífera al Conocimiento de la Geología de España*, Insi. Geo. y Minero de Esp, Madrid.

Laumonier, B., A. Autran, P. Barbey, A. Cheilletz, T. Baudin, A. Cocherie, and C. Guerrot (2004), Conséquences de l'absence de socle cadomien sur l'âge et la signification des séries pré-varisques (anté-Ordovicien supérieur) du sud de la France (Pyrénées, Montagne Noire), *Bull. Soc. Geol. Fr.*, *175*(6), 643–655.

Le Pichon, X., and J.-C. Sibuet (1971), Western extension of boundary between European and Iberian Plates during the Pyrenean orogeny, *Earth Planet. Sci. Lett.*, *12*(1), 83–88, doi:10.1016/0012-821X(71)90058-6.

Manatschal, G. (2004), New models for evolution of magma-poor rifted margins based on a review of data and concepts from West Iberia and the Alps, *Int. J. Earth Sci. (Geol. Rundsch.)*, *93*(3), doi:10.1007/s00531-004-0394-7.

Martinez-Peña, M., and A. Casas-Sainz (2003), Cretaceous–Tertiary tectonic inversion of the Cotiella Basin (southern Pyrenees, Spain), *Int. J. Earth Sci. (Geol. Rundsch.)*, *92*(1), 99–113, doi:10.1007/s00531-002-0283-x.

Marzoli, A., P. R. Renne, E. M. Piccirillo, M. Ernesto, G. Bellieni, and A. De Min (1999), Extensive 200-million-year-old continental flood basalts of the central Atlantic magmatic province, *Science*, *284*(5414), 616–618.

Masini, E., G. Manatschal, G. Mohn, J.-F. Ghienne, and F. Lafont (2011), The tectono-sedimentary evolution of a supra-detachment rift basin at a deep-water magma-poor rifted margin: The example of the Samedan Basin preserved in the Err Nappe in SE Switzerland, *Basin Res.*, *23*(6), 652–677, doi:10.1111/j.1365-2117.2011.00509.x.

Maurel, O., P. Monié, R. Pik, N. Arnaud, M. Brunel, and M. Jolivet (2008), The Meso-Cenozoic thermo-tectonic evolution of the Eastern Pyrenees: An Ar-40/Ar-39 fission track and (U-Th)/He thermochronological study of the Canigou and Mont-Louis Massifs, *Int. J. Earth Sci. (Geol. Rundsch.)*, *97*(3), 565–584.

McClay, K., J. A. Muñoz, and J. García-Senz (2004), Extensional salt tectonics in a contractional orogen: A newly identified tectonic event in the Spanish Pyrenees, *Geology*, *32*(9), 737–740, doi:10.1130/g20565.1.

McIntosh, K., H. van Avendonk, L. Lavier, W. R. Lester, D. Eakin, F. Wu, C.-S. Liu, and C.-S. Lee (2013), Inversion of a hyper-extended rifted margin in the southern Central Range of Taiwan, *Geology*, *41*(8), 871–874, doi:10.1130/G34402.1.

Meigs, A. J., and D. W. Burbank (1997), Growth of the south Pyrenean orogenic wedge, *Tectonics*, *16*(2), 239–258, doi:10.1029/96TC03641.

Meigs, A., J. Vergés, and D. W. Burbank (1996), Ten-million-year history of a thrust sheet, *Geol. Soc. Am. Bull.*, *108*(12), 1608–1625.

Mellere, D. (1993), Thrust-generated, back-fill stacking of alluvial fan sequences, south-central Pyrenees, Spain (La Pobla de Segur Conglomerates), in *Tectonic Controls and Signatures in Sedimentary Successions*, *Spec. Publ. Int. Ass. Sediment.*, vol. 20, edited by L. E. Frostick and R. J. Steel, pp. 259–276, doi:10.1002/9781444304053.ch14.

Mesalles, L., F. Mouthereau, M. Bernet, C.-P. Chang, A. Tien-Shun Lin, C. Fillon, and X. Sengelen (2014), From submarine continental accretion to arc-continent orogenic evolution: The thermal record in southern Taiwan, *Geology*, *42*(10), 907–910.

Metcalf, J. R., P. G. Fitzgerald, S. L. Baldwin, and J. A. Muñoz (2009), Thermochronology of a convergent orogen: Constraints on the timing of thrust faulting and subsequent exhumation of the Maladeta Pluton in the Central Pyrenean Axial Zone, *Earth Planet. Sci. Lett.*, *287*, 488–503.

Mohn, G., G. Manatschal, M. Beltrando, E. Masini, and N. Kusznir (2012), Necking of continental crust in magma-poor rifted margins: Evidence from the fossil Alpine Tethys margins, *Tectonics*, *31*, TC1012, doi:10.1029/2011tc002961.

Molnar, P., and J. M. Stock (2009), Slowing of India's convergence with Eurasia since 20 Ma and its implications for Tibetan mantle dynamics, *Tectonics*, *28*, TC3001, doi:10.1029/2008tc002271.

Montigny, R., B. Azambre, M. Rossy, and R. Thuizat (1986), K-Ar Study of cretaceous magmatism and metamorphism in the Pyrenees: Age and length of rotation of the Iberian Peninsula, *Tectonophysics*, *129*(1–4), 257–273, doi:10.1016/0040-1951(86)90255-6.

Morris, R. G., H. D. Sinclair, and A. J. Yelland (1998), Exhumation of the Pyrenean orogen: Implications for sediment discharge, *Basin Res.*, *10*, 69–85.

Mouthereau, F., and O. Lacombe (2006), Inversion of the Paleogene Chinese continental margin and thick-skinned deformation in the western foreland of Taiwan, *J. Struct. Geol.*, *28*(11), 1977–1993, doi:10.1016/j.jsg.2006.08.007.

Mouthereau, F., O. Lacombe, and J. Vergés (2012), Building the Zagros collisional orogen: Timing, strain distribution and the dynamics of Arabia/Eurasia Plate convergence, *Tectonophysics*, *532-535*, 27–60, doi:10.1016/j.tecto.2012.01.022.

Mouthereau, F., A. B. Watts, and E. Burov (2013), Structure of orogenic belts controlled by lithosphere age, *Nat. Geosci.*, *6*(8), 785–789, doi:10.1038/ngeo1902.

Muñoz, J. A. E. (1992), Evolution of a continental collision belt: ECORS-Pyrenees crustal balanced cross-section, in *Thrust Tectonics*, edited by K. McClay, pp. 235–246, Chapman and Hall, London.

Naylor, M., and H. D. Sinclair (2008), Pro- versus retro-foreland basins, *Basin Res.*, *20*, 285–303.
Olivet, J. L. (1996), La cinématique de la plaque Ibérique, *Bull. Cent. Rech. Explor. Prod. Elf Aquitaine*, *20*, 131–195.
Passchier, C. W. (1984), Mylonite-dominated footwall geometry in a shear zone, central Pyrenees, *Geol. Mag.*, *121*(5), 429–436, doi:10.1017/S0016756800029964.
Pik, R., B. Marty, J. Carignan, and J. Lavé (2003), Stability of the Upper Nile drainage network (Ethiopia) deduced from (U–Th)/He thermochronometry: Implications for uplift and erosion of the Afar plume dome, *Earth Planet. Sci. Lett.*, *215*(1–2), 73–88, doi:10.1016/S0012-821X(03)00457-6.
Plaziat, J. C. (1981), Late Cretaceous to late Eocene palaeogeographic evolution of southwest Europe, *Palaeogeogr. Palaeoclimatol. Palaeoecol.*, *36*, 236–320.
Poblet, J., J. A. Muñoz, A. Trave, and J. Serra-Kiel (1998), Quantifying the kinematics of detachment folds using three-dimensional geometry; application to the Mediano Anticline (Pyrenees, Spain), *Geol. Soc. Am. Bull.*, *110*(1), 111–125.
Rahl, J. M., S. H. Haines, and B. A. van der Pluijm (2011), Earth and planetary science letters, *Earth Planet. Sci. Lett.*, *307*(1–2), 180–190, doi:10.1016/j.epsl.2011.04.036.
Reston, T., and K. McDermott (2014), An assessment of the cause of the "extension discrepancy" with reference to the west Galicia margin, *Basin Res.*, *26*(1), 135–153, doi:10.1111/bre.12042.
Rocher, M., O. Lacombe, J. Angelier, B. Deffontaines, and F. Verdier (2000), Cenozoic folding and faulting in the south Aquitaine Basin (France): Insights from combined structural and paleostress analyses, *J. Struct. Geol.*, *22*(5), 627–645, doi:10.1016/S0191-8141(99)00181-9.
Roest, W. R., and P. S. Srivastava (1991), Kinematics of the plate boundaries between Eurasia, Iberia, and Africa in the North Atlantic from the Late Cretaceous to the present, *Geology*, *19*(June), 613–616.
Rosell, J., R. Linares, and C. Llompart (2001), El "Garumniense" prepirenaico, *Rev. Soc. Geol. Espana*, *14*(1–2), 47–56.
Rosenbaum, G., G. S. Lister, and C. Duboz (2002), Relative motions of Africa, Iberia and Europe during Alpine orogeny, *Tectonophysics*, *359*(1–2), 117–129, doi:10.1016/S0040-1951(02)00442-0.
Roure, F., and P. Choukroune (1998), Contribution of the Ecors seismic data to the Pyrenean geology: Crustal architecture and geodynamic evolution of the Pyrenees, in *The ECORS Pyrenean Deep Seismic Surveys, 1985–1994*, Mém. Soc. Géol. France, edited by B. Damotte, pp. 37–52.
Roure, F., P. Choukroune, X. Beràstegui, J. A. Muñoz, A. Villien, P. Matheron, M. Bareyt, M. Séguret, P. Camara, and J. Déramond (1989), ECORS deep seismic data and balanced cross sections: Geometric constraints on the evolution of the Pyrenees, *Tectonics*, *8*(1), 41–50, doi:10.1029/TC008i001p00041.
Rushlow, C. R., J. B. Barnes, T. A. Ehlers, and J. Vergés (2013), Exhumation of the southern Pyrenean fold-thrust belt (Spain) from orogenic growth to decay, *Tectonics*, *32*, 843–860, doi:10.1002/tect.20030.
Sainz, A. M. C., and C. Faccenna (2001), Tertiary compressional deformation of the Iberian Plate, *Terra Nova*, *13*(4), 281–288, doi:10.1046/j.1365-3121.2001.00355.x.
Savostin, L. A., J.-C. Sibuet, L. P. Zonenshain, X. Le Pichon, and M.-J. Roulet (1986), Kinematic evolution of the Tethys belt from the Atlantic Ocean to the Pamirs since the Triassic, *Tectonophysics*, *123*(1–4), 1–35, doi:10.1016/0040-1951(86)90192-7.
Schärer, U., P. de Parseval, M. Polvé, and M. de Saint Blanquat (1999), Formation of the Trimouns talc-chlorite deposit (Pyrenees) from persistent hydrothermal activity between 112 and 97 Ma, *Terra Nova*, *11*(1), 30–37, doi:10.1046/j.1365-3121.1999.00224.x.
Schettino, A., and E. Turco (2010), Tectonic history of the western Tethys since the Late Triassic, *Geol. Soc. Am. Bull.*, *123*(1–2), 89–105, doi:10.1130/B30064.1.
Schmitz, B., and V. Pujalte (2007), Abrupt increase in seasonal extreme precipitation at the Paleocene-Eocene boundary, *Geology*, *35*(3), 215–218, doi:10.1130/G23261A.1.
Séguret, M. (1972), Etude tectonique des nappes et séries décollées de la partie centrale du versant sud des Pyrénées, Caractère synsédimentaire, rôle de la compression et de la gravité, PhD thesis, Montpellier, 150 p.
Sibuet, J.-C., S. P. Srivastava, and W. Spakman (2004), Pyrenean orogeny and plate kinematics, *J. Geophys. Res.*, *109*, B08104, doi:10.1029/2003JB002514.
Sinclair, H. D., M. Gibson, M. Naylor, and R. G. Morris (2005), Asymmetric growth of the Pyrenees revealed through measurement and modeling of orogenic fluxes, *Am. J. Sci.*, *305*(May), 369–406.
Souriau, A., S. Chevrot, and C. Olivera (2008), A new tomographic image of the Pyrenean lithosphere from teleseismic data, *Tectonophysics*, *460*(1–4), 206–214, doi:10.1016/j.tecto.2008.08.014.
Srivastava, S. P., H. Schouten, W. R. Roest, K. D. Klitgord, L. C. Kovacs, J. Verhoef, and R. Macnab (1990), Iberian Plate kinematics—A jumping plate boundary between Eurasia and Africa, *Nature*, *344*(6268), 756–759, doi:10.1038/344756a0.
Srivastava, S. P., J. C. Sibuet, S. Cande, W. R. Roest, and I. D. Reid (2000), Magnetic evidence for slow seafloor spreading during the formation of the Newfoundland and Iberian margins, *Earth Planet. Sci. Lett.*, *182*(1), 61–76, doi:10.1016/s0012-821x(00)00231-4.
Stacey, J. S., and J. D. Kramers (1975), Approximation of terrestrial lead isotope evolution by a two-stage model, *Earth Planet. Sci. Lett.*, *26*(2), 207–221, doi:10.1016/0012-821X(75)90088-6.
Sutra, E., G. Manatschal, G. Mohn, and P. Unternehr (2013), Quantification and restoration of extensional deformation along the western Iberia and Newfoundland rifted margins, *Geochem. Geophys. Geosyst.*, *14*, 2575–2597, doi:10.1002/ggge.20135.
Teixell, A. (1998), Crustal structure and orogenic material budget in the west central Pyrenees, *Tectonics*, *17*(3), 395–406, doi:10.1029/98TC00561.
Urgeles, R., A. Camerlenghi, D. Garcia-Castellanos, B. De Mol, M. Garcés, J. Vergés, I. Haslam, and M. Hardman (2011), New constraints on the Messinian sealevel drawdown from 3D seismic data of the Ebro Margin, western Mediterranean, *Basin Res.*, *23*(2), 123–145, doi:10.1111/j.1365-2117.2010.00477.x.
Vacherat, A., F. Mouthereau, R. Pik, M. Bernet, C. Gautheron, E. Masini, L. Le Pourhiet, B. Tibari, and A. Lahfid (2014), Thermal imprint of rift-related processes in orogens as recorded in the Pyrenees, *Earth Planet. Sci. Lett.*, *408*(0), 296–306.
van Hinsbergen, D. J. J., R. L. M. Vissers, and W. Spakman (2014), Origin and consequences of western Mediterranean subduction, rollback, and slab segmentation, *Tectonics*, *33*, 393–419, doi:10.1002/2013TC003349.
Vauchez, A., C. Clerc, L. Bestani, Y. Lagabrielle, A. Chauvet, A. Lahfid, and D. Mainprice (2013), Preorogenic exhumation of the north Pyrenean Agly Massif (Eastern Pyrenees-France), *Tectonics*, *32*, 95–106, doi:10.1002/tect.20015.
Vergés, J. (1993), Estudi geològic del vessant sud del Pirineu oriental i central, Evolució cinemàtica en 3D, Universitat de Barcelona, Barcelona, 27 November.
Vergés, J., and J. A. Muñoz (1990), Thrust sequence in the southern central Pyrenees, *Bull. Soc. Geol. Fr.*, *VI*(2), 265–271, doi:10.2113/gssgfbull.VI.2.265.
Vergés, J., and J. García-Senz (2001), Mesozoic evolution and Cainozoic inversion of the Pyrenean rift, *Mém. Mus. Natl. Hist. Nat.*, *186*, 187–212.
Vergés, J., and M. Fernàndez (2012), Tethys–Atlantic interaction along the Iberia–Africa plate boundary: The Betic–Rif orogenic system, *Tectonophysics*, *579*, 144–172.

Vergés, J., H. Millán, J. A. Muñoz, M. Marzo, J. Cirès, T. Den Bezemer, R. Zoetemeijer, and S. Cloetingh (1995), Eastern Pyrenees and related foreland basins: Pre-, syn- and post-collisional crustal-scale cross-sections, *Mar. Petrol. Geol.*, *12*(8), 893–915.

Vergés, J., M. Fernàndez, and A. Martínez (2002), The Pyrenean orogen: Pre-, syn-, and post-collisional evolution, in *Reconstruction of the Evolution of the Alpine-Himalayan Orogen*, vol. 8, edited by G. Rosenbaum and G. Lister, pp. 55–74, Journal of the Virtual Explorer.

Vergés, J., E. Saura, E. Casciello, M. Fernàndez, A. Villaseñor, I. Jiménez-Munt, and D. Garcia-Castellanos (2011), Crustal-scale cross-sections across the NW Zagros belt: Implications for the Arabian margin reconstruction, *Geol. Mag.*, *148*(5–6), 739–761, doi:10.1017/S0016756811000331.

Vermeesch, P. (2004), How many grains are needed for a provenance study?, *Earth Planet. Sci. Lett.*, *224*(3–4), 441–451, doi:10.1016/j.epsl.2004.05.037.

Vermeesch, P. (2009), RadialPlotter: A Java application for fission track, luminescence and other radial plots, *Radiat. Meas.*, *44*(4), 409–410, doi:10.1016/j.radmeas.2009.05.003.

Vermeesch, P. (2012), On the visualisation of detrital age distributions, *Chem. Geol.*, *312-313*(C), 190–194, doi:10.1016/j.chemgeo.2012.04.021.

Vielzeuf, D., and J. Kornprobst (1984), Crustal splitting and the emplacement of Pyrenean lherzolites and granulites, *Earth Planet. Sci. Lett.*, *67*(1), 87–96, doi:10.1016/0012-821x(84)90041-4.

Vissers, R. L. M. (1992), Variscan extension in the Pyrenees, *Tectonics*, *11*(6), 1369–1384, doi:10.1029/92TC00823.

Vissers, R. L. M., and P. T. Meijer (2012a), Iberian Plate kinematics and Alpine collision in the Pyrenees, *Earth Sci. Rev.*, *114*(1–2), 61–83, doi:10.1016/j.earscirev.2012.05.001.

Vissers, R. L. M., and P. T. Meijer (2012b), Mesozoic rotation of Iberia: Subduction in the Pyrenees?, *Earth Sci. Rev.*, *110*(1–4), 93–110, doi:10.1016/j.earscirev.2011.11.001.

Whitchurch, A. L., A. Carter, H. D. Sinclair, R. A. Duller, A. C. Whittaker, and P. A. Allen (2011), Sediment routing system evolution within a diachronously uplifting orogen: Insights from detrital zircon thermochronological analyses from the south-central Pyrenees, *Am. J. Sci.*, *311*(5), 442–482, doi:10.2475/05.2011.03.

Wiedenbeck, M., P. Allé, F. Corfu, W. L. Griffin, M. Meier, F. Oberli, A. V. Quadt, J. C. Roddick, and W. Spiegel (1995), Three natural zircon standards for U-Th-Pb, Lu-Hf, trace element and REE analyses, *Geostandard. Newslett.*, *19*(1), 1–23, doi:10.1111/j.1751-908X.1995.tb00147.x.

Wrobel-Daveau, J.-C., J.-C. Ringenbach, S. Tavakoli, G. M. H. Ruiz, P. Masse, and D. Frizon de Lamotte (2010), Evidence for mantle exhumation along the Arabian margin in the Zagros (Kermanshah area, Iran), *Arab. J. Geosci.*, *3*(4), 499–513.

Yelland, A. J. (1991), *Thermo-Tectonics of the Pyrenees and Provenance From Fission-Track Studies*, Birbeck College, Univ. of London, London.